WORLD NUCLEAR ASSOCIATION

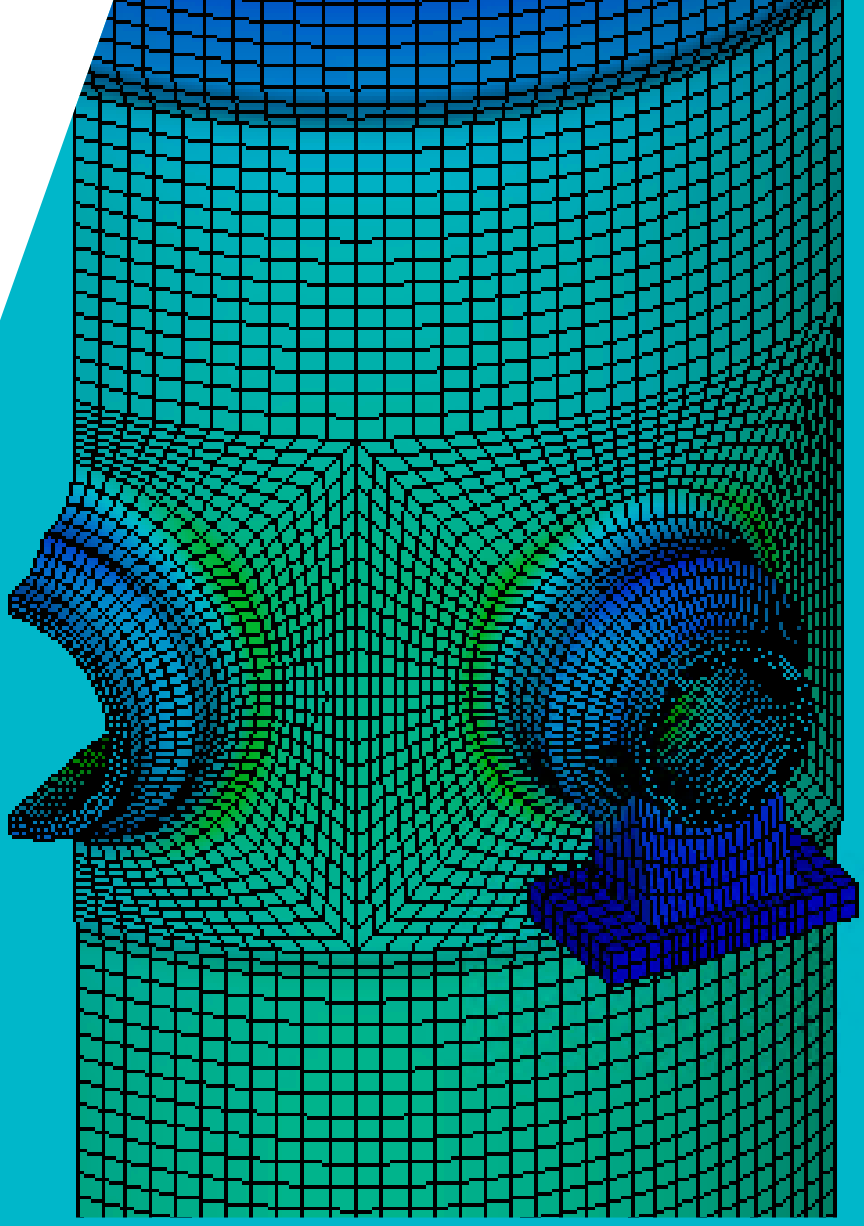

Non-Linear Analysis Design Rules

Part 3: Recommendations for Industrial Practices

Cooperation in Reactor Design Evaluation and Licensing – Mechanical Codes and Standards Task Force

Title: Non-Linear Analysis Design Rules
Part 3: Recommendations for
Industrial Practices
Produced by: World Nuclear Association
Published: July 2021
Report No. 2021/002

Cover Photo: Contour plot of a APR1400,
provided by KEPCO E&C by
Hyosub Yoon's team.

Contributors to the report

Project Coordinator

Ronan Tanguy, World Nuclear Association (United Kingdom)

Authors

Denis Pont, EDF (France)

Hadagali Shivakumar, ProSIM (India)

David Clarkson, Frazer-Nash Consultancy (United Kingdom)

Ludovic Jian, Naval Group (France)

Reviewers*

Aurélien Di Rienzo, Framatome (France)

Byung-Chan Na, World Nuclear Association (United Kingdom)

Cécile Petesch, CEA (France)

David Clarkson, Frazer-Nash Consultancy (United Kingdom)

Denis Pont, EDF (France)

Frédéric Beaud, EDF (France)

Hyosub Yoon, KEPCO E&C (South Korea)

Ludovic Jian, Naval Group (France)

Manuela Triay, Framatome (France)

Pierre Genette, EDF (France)

Ralf Trieglaff, TÜV Nord (Germany)

Roman Atroshenkov, Rosatom (Russia)

Stéphane Marie, Framatome (France)

Acknowledgements

The CORDEL Secretariat of the World Nuclear Association would like to convey its gratitude to their colleagues Richard Petrie and Stephen Tarlton for their expertise, patience, and diligence in respectively designing and editing this report.

* Alphabetical order

Foreword

The Cooperation in Reactor Design Evaluation and Licensing Working Group (CORDEL) of the World Nuclear Association (WNA) was established in 2007 to promote the development of a worldwide nuclear environment where internationally accepted standardized reactor designs can be deployed globally without major design changes. In practice, this would mean that safety evaluations of a reactor design and generic design certification approved by a recognized competent authority would be acceptable in other countries.

The CORDEL Mechanical Codes and Standards Task Force (MCSTF) was set up in 2011 and started to collaborate closely with the Standards Development Organizations Convergence Board (SDO CB) and the Codes and Standards Working Group of the Multinational Design Evaluation Programme (MDEP) on the international convergence of mechanical codes and standards related to the design of nuclear power plant components important to safety. The MCSTF's collaboration with regulators is now through the Committee on Nuclear Regulatory Activities' (CNRA) Working Group on Codes and Standards of the OECD/Nuclear Energy Agency. The MCSTF has worked to date principally in three areas: qualification of non-destructive examination personnel; fatigue analysis and design rules; and non-linear analysis design rules.

In the area of non-linear analysis design rules, the topics identified by the MCSTF for investigation with a view to harmonizing different approaches are: review and comparison of the current code requirements in non-linear analysis for different failure modes (plastic collapse, plastic instability, local failure and buckling) and some degradation mechanisms (fatigue, plastic shakedown) (Part 1); definition of international benchmark problems to compare the existing non-linear analysis practices and assessment of the benchmark results (Part 2); and development of harmonized recommended industrial practices (Part 3).

This report is Part 3 of the series of reports on the non-linear analysis design rules.

Based on the findings from and critical assessment of the Part 2 benchmark exercise outcomes, this report provides recommendations for industrial practices in non-linear analysis.

Abbreviations and acronyms

AFCEN	French Association for Design, Construction, and In-Service Inspection Rules for Nuclear Island Components (Association française pour les règles de conception, de construction et de surveillance en exploitation des matériels des chaudières électro-nucléaires)
ASME	American Society of Mechanical Engineers
ASN	French Nuclear Regulator (Autorité de Sûreté Nucléaire)
BPVC	Boiler & Pressure Vessel Code
CEA	French Alternative Energies and Atomic Energy Commission (Commissariat à l'énergie atomique et aux énergies alternatives)
CNRA	Committee on Nuclear Regulatory Activities
CORDEL	Cooperation in Reactor Design Evaluation & Licensing
EN	European Standard
EDF	Electricité de France
KEPCO-E&C	Korea Electric Power Corporation - Engineering and Construction
MCSTF	Mechanical Codes & Standards Task Force of CORDEL
MDEP	Multinational Design Evaluation Programme
NEA	Nuclear Energy Agency
OECD	Organisation for Economic Co-operation and Development
RCC-M	French Design and Construction Rules for the Mechanical Components of PWR Nuclear Islands (Règles de Conception et de Construction des Matériels Mécaniques des Ilots Nucléaires REP)
RCC-MRx	French Design and Construction Rules for the Mechanical Components of High Temperature, Experimental and Fusion Nuclear Installations (Règles de Conception et de Construction des Matériels Mécaniques des Installations Nucléaires Hautes Températures, Expérimentales et de Fusion)
RSE-M	French In-Service Inspection Rules for Mechanical Components of PWR Nuclear Islands (Règles de Surveillance en Exploitation des Matériels Mécaniques des Ilots Nucléaires REP)
SDO	Standards developing organization
SDO CB	Standards Development Organizations Convergence Board
WNA	World Nuclear Association
WRC	Welding Research Council

Technical nomenclature

CAD	Computer assisted design
CUF	Cumulative usage factor
CPU	Central processing unit
EVP	Extreme value pairing
FE	Finite element
FEA	Finite element analysis
FSRF	Fatigue strength reduction factor
FUF	Fatigue usage factor
HTC	Heat transfer coefficient
MCL	Main coolant line
PTP	Peak-to-peak
PUF	Partial usage factor
SCL	Stress classification line
SCF	Stress concentration factor
UTS	Ultimate tensile strength
C	RCC-M kinematic hardening modulus
γ	RCC-M recall coefficient for back stress tensor
$\Delta\varepsilon_t$	Elastic-plastic equivalent strain range
E	Young's modulus
e	Element thickness
E_α	Thermal expansion coefficient
E_a	Representative elastic modulus
E_c	Reference modulus of elasticity
E_{mod}	Elastic modulus correction factor
F	Peak stress
κ	Thermal diffusivity
K_e	Fatigue plasticity correction factor
$K_{e,eq}$	Weighted average of K_e^{ther} and K_e^{mech}
K_e^{ther}	RCC-M thermal plasticity correction factor
K_e^{mech}	RCC-M mechanical plasticity correction factor
ν	Poisson's ratio
P	Primary stress
P_b	Primary bending stress intensity

P_l	Primary local membrane stress intensity
P_m	Primary general membrane stress intensity
Q	Secondary stress
$R_{P0.2}$	0.2% offset yield strength
r	Radius
S_{alt}	Pseudo-elastic stress range
S_m	Design stress intensity
S_n	Primary-plus-secondary stress intensity range
S_N	Reversed alternating stress
S_p	Primary-plus-secondary-plus-peak (total) stress intensity range
S_p^{mech}	Total stress intensity range arising due to mechanical loads
S_p^{ther}	Total stress intensity range arising due to thermal loads
S_r	Alternating stress amplitude
σ	Stress
σ_{eq}	Equivalent stress
σ_i	Principal stress
σ_{ij}	Continuum FEA stress
σ_b	Bending stress tensor
$\sigma_{ij,b}$	Bending stress distribution
σ_l	Linear stress tensor
σ_m	Membrane stress tensor
$\sigma_{ij,m}$	Membrane stress distribution
σ_y	Initial tensile yield strength
T	Temperature
T_w	Weighted average service temperature
t	Time
X	Back stress tensor

Contents

List of tables

List of figures

Executive summary

This report is the final part (Part 3) of a series of reports aimed at identifying a more harmonized approach in using non-linear analysis methods.

Major pressure vessel and piping codes design rules, nuclear and non-nuclear, are based on linear elastic methods associated with stress classification in primary (for load control), secondary (for strain control) and peak stresses (for thermal shocks). This stress classification is only straightforward to apply in simple cases, such as a cylindrical shell subjected to axisymmetric quasi-static loads. When the geometry or the loads become more complex, such classifications are not applicable, so a large part of stress is considered as primary which is extremely conservative. In such cases, non-linear analysis methods are employed. Comparison of these methods has shown that many different approaches are currently used within the industry, which gives rise to discrepancies in the analysis and assessment of designs.

Following an initial comparison of non-linear analysis design rules in nuclear mechanical codes and standards (Part 1 of this series of reports), two benchmark problems were specified for two typical nuclear components (Part 2a of this series). The first benchmark problem was based on a large Class 1 low alloy steel vessel nozzle under pressure and piping loads where the aim was to analyse elastic stress, plastic collapse, plastic instability, and local failure. The second benchmark problem was based on a Class 1 reinforced stainless steel piping tee under cyclic pressure and thermal loads to perform fatigue assessment. These two benchmarks only considered non-cracked components outside of creep regime.

This Part 3 report presents recommendations in support of international harmonization of non-linear analysis methods following the assessments and findings of the previous report (Part 2b) in the series.

Linear mechanical analysis, elastic fatigue analysis and plastic fatigue analysis are covered within this report with several recommendations provided for each one. Detailed recommended approaches are proposed for the following sub-topics as mooted in Part 2b:

- Resolving stress tensors along the stress classification line.
- Selection of the section for study (approaches for discontinuities and singularities).
- Guidelines for linearization procedures.
- Finite element analysis best practices (2D & 3D, meshing, post-processing, and assessment).
- Deriving true stress-strain curves from material data.
- Selecting the value of flow stress for use in limit load.
- Combining cyclical thermal and mechanical loads to obtain peak stresses.
- Accurately calculating the elastic-plastic concentration factor K_e.
- Calculating the fatigue usage factor.
- Selecting the most suitable equivalent strain range for the characterization of fatigue damage.

1. Introduction

This report provides recommendations for industrial practices in the field of non-linear analysis design rules based on recent analyses and findings obtained by the previous activities of the CORDEL Mechanical Codes and Standards Task Force.

Benchmark problems were specified in Part 2a of this series of reports (1) in which the following two typical nuclear components were selected for international benchmarking:

- A large Class 1 low alloy steel vessel nozzle under pressure and piping loads for the first benchmark problem to analyse plastic collapse, plastic instability, and local failure.
- A Class 1 reinforced stainless steel piping tee under cyclic pressure and thermal loads for the second benchmark problem to analyse fatigue.

The results from these benchmarks were compared and assessed in Part 2b of this series of reports (2) to identify the areas in which a consensus appears to be emerging for non-linear analysis methods and those in which further discussions are required to resolve differences between approaches. Recommendations for analysts performing non-linear analysis (mechanical analysis, elastic fatigue analysis and plastic fatigue analysis) and implementing damage assessment procedures notably for areas which were identified in the Part 2b report (2) as lacking guidance within the design codes.

Before comparison and assessment of non-linear results, the benchmarks proposed initial analyses with linear approaches. This approach is consistent with industry practice, as non-linear approaches are undertaken if the linear analyses are unable to fulfil codified criteria. The prior report (2) provides results alongside general comments and questions for such analyses.

Mechanical analyses aim to study the behaviour of components undergoing mechanical and thermal loads. The types of damage that can result from such loads are listed in international codes and standards such as ASME, RCC-M, EN *etc*. and range from excessive deformation, plastic instability, elastic or elastic-plastic instability, progressive deformation, fatigue, creep, to fast fracture.

The mechanical justification is assumed to be performed according to these standards. In the standards' design chapters, damages to be avoided are described and general procedures are provided based on stress analysis and criteria. Additional criteria are provided for local failure, local pressure (bolted heads), maximum shear stress, *etc*.

2. Linear mechanical analysis recommendations

In linear analyses, the mechanical features to be assessed are stresses or stress variations. Standards for the nuclear industry define three categories of stress: membrane stress; membrane + bending stress; and peak stress. These stresses are typically associated with certain types of material damage:

- Membrane stresses and membrane + bending stresses for excessive deformation and plastic instability.
- Membrane + bending stress variations for progressive deformation.
- Membrane + bending stress variations and peak stress variations for fatigue analysis, which is performed after progressive deformation checks.

The membrane stress and the bending stress are obtained by a linearization procedure which considers the material's whole thickness. The peak stress, on the other hand, is located on the material's surface and therefore the mesh density is of greater importance.

Specific inequalities comparing stress results with allowable limits (criteria) must be checked for each type of damage.

The accuracy of stress magnitudes depends on transient descriptions and time discretization. Close attention must therefore be paid to these two aspects.

The analysis methodology also depends on:

- The type of structure (shells, pipes, connecting parts, bolts, *etc*.). In following sections, specificities of pipes, bolts, connecting parts are not discussed.
- The safety class of the component studied.
- The situations undergone by the component (each situation is described in terms of pressure, forces, moments, thermal transients).

This report is focused on analyses concerning excessive deformation and plastic instability (plus decohesion criteria). The specificities of creep and fast fracture are not discussed in the report.

General recommendations for analyses using a finite element method are provided for the following tasks:

- Engineering practices for finite element analysis (FEA) stress assessment (mesh, boundary conditions, loads *etc*.).
- Post-processing of FEA stresses.
- Damage assessment, stress classification and criteria.

2.1 Stress calculation

Depending on the complexity of geometry and loads, the stresses can be assessed either with analytical formulae (Roark's *Formulas for Stress and Strain* for example) or with dedicated software which uses mechanical elastic equilibrium equations. A stress calculation software typically works using FEA. This technique enables the user to work with a wide range of geometries upon which various mechanical loads can be applied thereby allowing them to extract relevant results such as displacements and stresses.

FEA software is also capable of calculating the thermal fields in the geometries it analyses and the resulting loads.

2.1.1 Geometry

The shape of the part must generally be defined before modelling to account for fabrication tolerances and potential shape modifications during its lifetime that could arise from phenomena such as corrosion. Standards such as RCC-M provide guidance for defining the actual thickness to be used for stress analysis.

The finite element model must reproduce the geometry of the design, with a level of detail consistent with the behaviour being considered, the expected results (local stresses, stresses on the skins, membrane stresses or bending stresses) and considering minor and major discontinuities.

Splitting a component into several distinct zones of calculation is often recommended. The interactions between these zones must be correctly considered with regard to displacements or/and forces (see Section 2.1.3 on boundary conditions). The boundaries of the model must be chosen prudently to avoid any impact on the behaviour of the zone being studied.

The choice between a three-dimensional (3D) and two-dimensional (2D) approach with the appropriate assumptions (plane stress, axisymmetric option, plane strain or generalised plane strain) is another crucial factor. The designer must find a compromise between industrial calculations with reasonable CPU times and sophisticated calculations producing very precise and detailed results. Three-dimensional studies have become more commonplace nowadays however, thanks to advances in computing capabilities.

Two-dimensional calculations present drawbacks such as having to hypothesize the stress/strain in the third (absent) direction, the impossibility to apply some loads specified with all tensor components and the necessity to correctly approximate sections of the geometry. In Benchmark 1 for example, the radius of the vessel is corrected to adjust the level of 2D hoop stresses to the expected level of 3D hoop stresses. The ellipsoidal connection between vessel and nozzle in 3D is also approximated by a circular connection in 2D.

The advantages of three-dimensional model are the ability to apply a complete tensor (forces/moments) and use realistic shapes with fewer assumptions. 3D models present two main drawbacks however, firstly the size of the resulting model (which comprises a higher number of elements and nodes) which may require optimization. The second drawback is that obtaining results can be more difficult as the selection of an area to analyse is more complicated (a plane and then a line must be chosen) as code values are based upon averages through a thickness of the material.

It is therefore recommended that two-dimensional analysis should be used when the geometry is simple (*e.g.*, axisymmetric) and the applied forces only have two components. Three-dimensional analysis should be used for all other analyses as it allows for more realistic simulations and provides more accurate results that make up for its longer computation and more challenging interpretation of results. It is also recommended that symmetry conditions should be used when creating the FE model when possible.

2.1.2 Mesh

A typical FEA software offers a large choice of types of elements: solid elements, shell elements, beams *etc*. The choice of elements must be consistent with their domain of validity (*i.e.*, ratio thickness/radius for shells) and with the behaviour of the structure (*e.g.* in case of bending). The mesh density must also be commensurate with the variation of displacements/rotations and the stress gradients. The user can check if their choice of elements was appropriate once calculations are completed by examining post-processing results.

The mesh density must therefore be increased when approaching (and at) discontinuity zones where stress concentrations occur. The discretization through the thickness must be fine enough to capture stress gradients present due to bending (several elements are required even for thin structures).

Sensitivity analyses can be carried out to control variations in calculated stresses. Some software includes tools to estimate error and to increase mesh quality where required.

In the case of thermal transient calculations, the size of elements close to the surfaces must be small enough to reproduce thermal gradients throughout the thickness. The time discretization and time integration scheme must be chosen to provide thermal field stability to avoid temperature oscillations (Peclet or Fourier number). This choice is particularly relevant for calculations performed as part of progressive deformation and fatigue analyses.

2.1.3 Boundary conditions

As the model only represents part of the component studied, boundary conditions must be defined in order not to alter the quality of results. The designer must pay attention to the location of boundaries and how they are defined (imposed displacements, forces, kinematic conditions). In Benchmark 1 for example, the pipe boundaries must be far enough away from the discontinuity (thickness variation) and must account for pipe continuity.

For axisymmetric geometries, the distance between boundary conditions and discontinuities must be greater than $\alpha\sqrt{re}$ (where α: coefficient; r: radius and e: thickness) to account for the damping of displacement.

2.1.4 Material properties

The following material properties are required for the mechanical calculations (static assumptions) for each material:

- Young's modulus.
- Poisson's ratio.
- Thermal expansion coefficient (in case of previous thermal calculation).

Additional material properties are required for the thermal calculations:

- Thermal properties (conductivity coefficient and heat capacity coefficient) and density for each material.
- Heat exchange coefficients for each surface associated with temperature of the external medium.

The designer must also set the temperature within the material properties. In the cases of loads such as pressure or forces, the temperature (room temperature or maximum temperature) considered for Young's modulus will not affect stress results. With multiple materials however, stress redistributions due to differences of stiffness may depend on temperature.

2.1.5 Combination of actions

The calculations are performed for each elementary load. The practice is then to combine the results of elementary loads to obtain results for the situations being studied (design conditions, fault conditions, and test conditions).

2.2 Post-processing

Once the calculations are completed, the software presents the resulting displacement fields and stress fields (tensor components), which can be plotted as deformed shapes and displacement/stress distributions. A global analysis of the results is required to check the quality of results.

Stresses are then locally post-processed and analysed as described in the following sub-sections.

2.2.1 Stress components, equivalent stress

Most codes and standards define rules to extract stress components and to calculate equivalent stresses.

At each point, the stress tensor is described by three normal stress components and three shear stress components. For a given section supported by a segment line, the distribution of each stress component is extracted. The average stress (membrane) and the linear stress are then calculated for each stress component. The bending stress component is obtained by subtracting membrane stress components from linear stress components.

The membrane stresses (denoted P_m or P_L) and membrane + bending stress (denoted (P_m or P_L) + P_b) are expressed as equivalent stresses. These equivalent stresses enable a 3x3 tensor stress state to be represented by a scalar and are calculated from linearized stress components using one of the two following methods: octahedral shear method or maximum shear method. The corresponding equivalent stresses used in codes and standards are: Tresca stress and von Mises stress. It should be noted that the Tresca criterion is conservative compared to von Mises criterion (the maximum difference is equal to $1 - \sqrt{3}/2 \approx 13\%$) but is in line with classical dimensioning formulae of pressurized components.

The equivalent stress is expressed in relation to σ_i (principal stresses) in the principal coordinate system as follows:

- According to Tresca:

$$\sigma_{eq,Tresca} = Max(|\sigma_1 - \sigma_2|, |\sigma_2 - \sigma_3|, |\sigma_1 - \sigma_3|)$$

Equation 1

- According to von Mises:

$$\sigma_{eq,VM} = \sqrt{\frac{1}{2}[(\sigma_1 - \sigma_2)^2 + (\sigma_2 - \sigma_3)^2 + (\sigma_1 - \sigma_3)^2]}$$

Equation 2

2.2.2 Stress classification lines

Defining stress classification lines (SCLs), sometimes referred to as cross-sections or path, is a crucial step because the stresses extracted in these SCLs are directly compared to allowable stresses (criteria).

The SCLs outside of discontinuity zones are line segments that are perpendicular to the median surface of the wall. In the discontinuity zones, they are the shorter lines which join the inner and outer surfaces (possible failure locations).

In all relevant zones, line segments must be selected to include maximum stress values (membrane and membrane + bending stresses). Sensitivity analysis could consequently be required. For example, the locations of maximum peak stress (fatigue), maximum membrane stress and maximum membrane + bending stress may be different. Certain special locations like singularities must be treated with caution. If the location of the SCL affects some components of the stress tensor by numerical disturbance, sensitivity analyses are then helpful to take relevant parameters into account: realistic shape, post-processing methods (values at nodes or at integration points). The specific case of an axisymmetric shell/flat head (3) shows that an average stress calculated using FEA through the thickness and perpendicular to a SCL containing a sharp singularity is affected by a numerical disturbance.

It is therefore recommended that FEA should only be used to establish trends approaching a discontinuity as any attempt to obtain results at the discontinuity will not succeed.

2.2.3 Linearization of stresses

Linearization guidelines in RCC-MRx (RB 3224) provide classical formulae for the linearization of all stress components (see below). RCC-M (B 3232.5) gives a procedure for the linearization of each stress component (with a remark concerning the radial stress which could be not linearized due to the pressure on the inner skin).

ASME Section VIII-2 (Annex 5-A) describes detailed procedures for the location of SCLs and the linearization. Some advice is provided for through-thickness stress and shear stresses.

The following formulae are consistent with the three standards mentioned above.

The membrane stress tensor σ_m along the line segment (x coordinate) is determined as:

$$\sigma_m(x) = \frac{1}{e}\int_{-e/2}^{+e/2} \sigma(x).dx$$

Equation 3

The bending stress tensor $\sigma_b(x)$ is determined as:

$$\sigma_b(x) = \frac{12x}{e^3}\int_{-e/2}^{+e/2} \sigma(x).xdx$$

Equation 4

The maximum bending stress on the skins is equal to:

$$\sigma_b(e/2) = \frac{6}{e^2}\int_{-e/2}^{+e/2} \sigma(x).xdx$$

Equation 5

Then the linear stress tensor along the line segment is equal to:

$$\sigma_l(x) = \sigma_m(x) \pm \sigma_b(x)$$

Equation 6

2.3 Stress analysis

The classification of stresses is a crucial step to be performed by the designer, according to the type of damage analysed, with the application of criteria on elastic stresses as specified in codes and standards. The classification of stresses accounts for the difference between the elastic behaviour and the real behaviour of the material, depending on the kind of load (imposed force, imposed displacement or imposed strain).

2.3.1 Stress classification

There is no need to apply any stress classification when the justification of the component uses experimental tests or an elastic-plastic analysis (see RCC-M criteria) (4), which represents the real behaviour of the structure as closely as possible.

The specificity of the elastic analysis is that the behaviour considered differs from real analysis when the effect of loads exceeds the limit of proportional behaviour. This difference depends on the kind of imposed deformations or imposed loads (weight, pressure, forces). An intermediate case exists with an imposed displacement to the neighbouring structures presenting a stiffness and acting on the considered component according to their rigidity as a spring.

A primary stress is any normal stress or shear stress resulting from the application of a load (weight, pressure, force) onto a material. These stresses appear to balance the loads as expected according to the laws of equilibrium of external and internal forces and moments. Primary stresses are defined as the fraction of the total stress which does not disappear after small permanent deformation; they remain within the material in the event of plastic deformation. The primary stress represents the fraction of total stress to be limited regarding excessive deformation and plastic instability.

Secondary stresses on the other hand, are normal stresses or shear stresses which develop because of constraints applied by adjacent materials or by self-constraint of the material. These

stresses are defined as the fraction of the total stress which can disappear after a small permanent deformation. They correspond to stresses resulting from imposed deformation (compatibility of strains, thermal strains, displacements).

The stress tensors determined by analysis shall be classified under:

P_m: general primary membrane stress

P_L: local primary membrane stress

P_b: primary bending stress

Q: secondary stress

F: peak stress

Then, for each criteria level 0, A, B, C and D, a limit is imposed on the stress intensities corresponding to each of these categories.

The stress classification depends on the kind of load and on the location of the zone studied, as detailed in codes and standards (RCC-M table B3231.7; ASME III-A table XIII-2600-1). The general principles are similar across codes and standards, but some differences may exist in specific cases.

In case of doubt regarding the classification, it is recommended that a conservative approach be taken and that the stress be considered as primary.

In Benchmark 1, which is a general configuration, the primary stresses to be analysed are:

- Internal pressure
  - Main vessel
    - Current zone: membrane stress (P_m)
    - Vicinity of nozzle: membrane stress (P_L)
  - Nozzle
    - Reinforcement zone: membrane stress (P_m)
    - Discontinuity reinforcement/pipe: membrane stress (P_L)
  - Pipe: membrane stress (P_m)
- External forces (from pipe)
  - Main vessel
    - Current zone: membrane stress (P_m)
    - Vicinity of nozzle: membrane stress (P_L) and bending stress (P_b)
  - Nozzle
    - Reinforcement zone: membrane stress (P_L) and bending stress (P_b)
    - Discontinuity reinforcement/pipe (P_L)
  - Pipe: membrane stress (P_m) and bending stress (P_b)

2.3.2 Stress criteria

The following stresses must be assessed for excessive deformation and plastic instability:

- General primary membrane stress (outside of gross discontinuity areas): P_m
- Local primary membrane stress intensity limits (in areas of gross discontinuity with conditions on the size of the zones where stresses exceed $1.1S_m$): P_L
- General or local primary membrane plus primary bending stress intensity limits: P_m (or P_L) + P_b

The inequalities to check (Class 1 components) for level 0 criteria (design level) are as follows:

- $P_m \leq S_m$
- $P_L \leq 1.5S_m$
- $P_m (or\ P_L) + P_b \leq 1.5S_m$

With S_m being the allowable basic stress at design temperature.

The designer must also check several special limitations (bearing loads, pure shear, triaxial stresses, *etc*.). Regarding the risk of decohesion, the algebraic sum of the three primary principal stresses ($\sigma_1 + \sigma_2 + \sigma_3$) shall not exceed $4S_m$. This criterion has been analysed in Benchmark 1. Note that in a current zone with a biaxial stress state (*i.e.*, on surfaces), this triaxiality criterion (combined with primary membrane + bending stress criteria) is always verified.

3. Plastic analysis recommendations

In this section, recommended practices for plastic analysis are described. The steps that must be considered before performing an engineering simulation using numerical methods should be revisited. Careful modelling and interpretation of results are therefore essential at this stage.

Multiple codes (ASME, RCC-M *etc*.) propose three methods with associated criteria to prevent the plastic instability of vessels: the elastic stress analysis criterion, the limit load analysis criterion, and the elastic-plastic stress criterion. In the elastic stress analysis, the calculated stresses are categorized into primary, secondary and peak stresses, which are all limited by introducing the allowable values (see Section 2). The limit load analysis assumes the elastic-perfectly plastic material property and a small deformation of vessels, but no gross plastic deformation. Selecting a suitable deformation parameter can prove challenging, especially when multiple loads are acting on the vessels. In contrast, the elastic-plastic stress analysis, which directly considers the actual material and the geometric nonlinear properties of the vessels, may result in gross plastic deformation before structural plastic collapse. The mechanical behaviours of vessels and the load carrying of vessels in the elastic-plastic stress analysis are more practical than those in the other two methods.

3.1 Plastic collapse

Plastic collapse methods are employed to determine the failure load in a material. These methods, also known as limit analysis, are particularly important for piping structures which can present exceptional strain conditions. These methods are used to detect the beginning of plastic behaviour which causes overall structural instability and the onset of gross plastic deformation; from this point onwards, the material exhibits a non-linear response to linear loading. Plastic collapse load is calculated from elastic-plastic material properties using small displacements and small strains. A plastic collapse analysis, as defined in the ASME BPVC (5), uses a multi-linear representation of the material's constitutive behaviour. The inclusion of strain hardening within this analysis, as well as large displacement effects, leads to a more faithful representation of reality.

3.1.1 Limit load method (critical load 1)

A limit load analysis, as defined in the ASME BPVC (5), is often referred to, somewhat misleadingly, as a lower-bound analysis. Its origin lies in the days of hand calculations and embodies the assumptions of small displacements and an elastic-perfectly plastic material model.

The limit load is the maximum load that a structure can safely carry. It is the load at which the structure is in a state of incipient plastic collapse. As the load on the structure increases, the displacements increase linearly in the elastic range until the load attains the yield value. The load-displacement response becomes non-linear beyond this point and the plastic or irreversible part of the displacement increases steadily with the applied load. Any load above the limit will lead to the formation of plastic hinges within the structure.

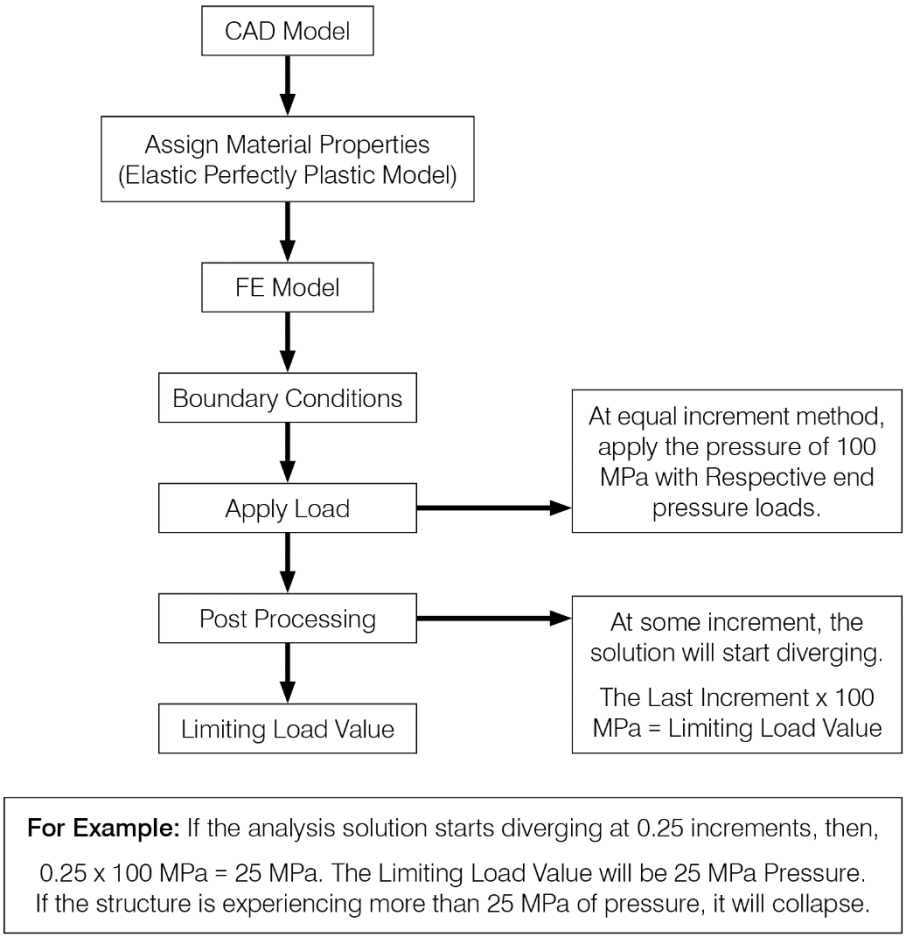

Figure 1. Recommended approach for the limit load method

From the benchmark results assessment (2) the differences in limit load values given by the 10 contributors are within 5% of each other.

Figure 1 presents the recommended approach for the limit load evaluation, (the final pressure of 100 MPa is given as an example). If all the loads are applied in increments (assuming a elastic-perfectly plastic model), when the deformation reaches its limit the solution will start to diverge. The same results should be obtained by all analysts when using the method of finding limit load value regardless of their analysis software. In order to determine the allowable load, the limit load must be reduced depending on the codes and standards' corresponding safety factors.

3.1.2 Double slope method (critical load 2)

A load-deflection curve is plotted with load P along the ordinate and deflection δ along the abscissa. The angle that the linear part of the load-deflection curve forms with the ordinate is denoted θ. A second line, the collapse limit line, is drawn through the origin so that it makes an angle $\varphi = \tan^{-1}(2\tan\theta)$ with the ordinate. The collapse load is the load at the intersection of the load-deflection curve and the collapse limit line as shown in Figure 2.

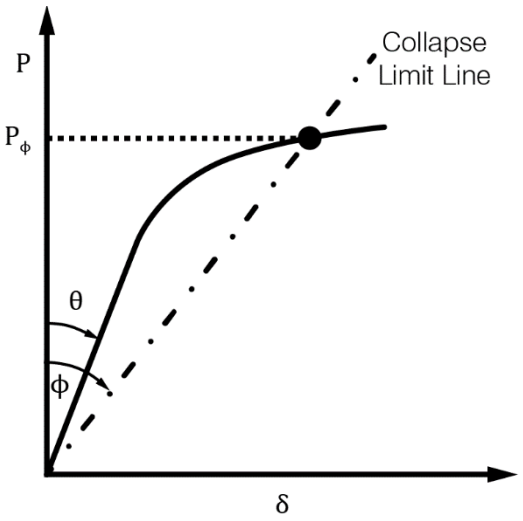

Figure 2. Double slope method

The elastic-plastic material model should be used to perform the plastic analysis. The selection of nodes for the plot is an important factor as the node which experiences the maximum displacement can be taken for the plot.

3.1.3 Maximum strain 0.5% (critical load 3)

The plastic collapse load can alternatively be obtained by keeping the local strain limit as 0.5%, *i.e.* when the applied load causes 0.5% strain in the model, the structure may collapse. This 0.5% criterion is not codified but was used in the benchmarks in the previous report (1). The selection of the strain component (interpretation of results) is an important factor here. In this report, the equivalent plastic strain was chosen for the plastic collapse load analysis. It should be noted that the 0.5% maximum local strain criterion is a severe numerical practice, without a direct link with plastic collapse, which is a global behaviour.

The elastic-plastic analysis can lead to a stronger ability to resist the failure than the limit load analysis because the latter is not true stress analysis due to the assumption of elastic-perfectly plastic material. The results provided by critical load 1 and critical load 2 approaches are similar however, when material properties are consistent. The complete elastic-plastic stress analysis is more practical and instructive than the limit load analysis and stress categorization method for the design of vessels, though the calculation cost of the complete elastic-plastic stress analysis is comparatively high.

3.1.4 Plastic collapse recommendations

The following recommendations for plastic analysis are therefore made:

- $R_{P0.2}$ should be considered as the value of flow stress to be used for the critical load 1 method, consistent with elastic-plastic methods.
- The von Mises stress criterion should be used for the yield criteria (it is compulsory for non-linear FEA calculations).
- Engineering stress-strain should be used for the collapse load for consistency with the small displacement/strain assumption. It should be noted however that the engineering stress-strain curve and the true stress-strain curve coincide for small strains.

- The finite element types should be carefully chosen, so that they can match the non-linear behaviour. Linear elements are generally not recommended.
- The location of maximum strain can be taken to determine the collapse load. It should be noted that this is geometry and mesh dependent and has not been codified.

3.2 Plastic instability

Several failure modes are considered in the ASME codes (5) (6) (7) for pressure vessels and piping. One of these failure modes is plastic instability. This failure mode is defined as the pressure at which the components/structures approach dimensional instability (large deformation), *i.e.*, unbounded displacement for a small increment in the applied load.

For most engineering steels, a non-uniform deformation field, called plastic instability, starts to develop just after a maximum load. Estimating the ultimate load (*e.g.*, internal pressure) that the component can withstand is useful for design and to assess its fitness for service. The ultimate load is defined as the load or load combination for which the component approaches dimensional instability (plastic instability), *i.e.* unbounded displacement for a small increment in the applied load.

When estimating the ultimate load or a load combination, both the true stress-strain curve and geometrical non-linearity must be considered in the analysis. This is only necessary when performing a non-linear analysis; this assumption is not needed for limit load analysis as the behaviour goes directly from linear to numerical collapse. The plastic limit load method uses a different approach and makes use of infinitesimal strain theory instead.

3.2.1 Plastic limit load

The limit load can be obtained with a similar approach to that shown in Figure 1, with an appropriate flow stress. The appropriate choice for the yield function depends on the material; von Mises and Tresca yield functions are used for metallic materials for example. Unlike Tresca, the von Mises yield function does not include any singularities in its formulation, therefore making it more suitable for numerical analysis. It should be noted that some codes propose a definition of the appropriate flow stress to be used.

3.2.2 Plastic instability load

An industrial method is to perform elastic-plastic calculation until plastic instability, which is detected by numerical divergence corresponding to a high level of plasticity and shape modification. This method enables analysts to assess margins preventing plastic instability. This kind of elastic-plastic calculation must account for large displacements, large strains and for the true stress-strain curve.

The true stress-strain material model with elastic-plastic analysis must be used to find the allowable loads. The true stress-strain curve, which is based on instantaneous stress classification line area and length, will give a close enough approximation for the limit load value. A conservative assessment of the plastic instability load can be obtained by limiting the maximum strain to 5% or 10%. Like the maximum strain 0.5% method for plastic collapse, once the equivalent plastic strain reaches 5%, the applied load will be taken to be the allowable load for the structure. The 10% maximum strain method is also applied in similar fashion to obtain the allowable loads. As discussed in Part 2b (2), the limit load method will provide the lesser value

for the allowable load compared to the other two methods. However if the stress-strain is consistent with the yield stress used in the limit analysis, then it will provide the opposite result as shown in the additional benchmark calculations provided by EDF (2). It should be noted that strain-based criteria are influenced by the location of the strain.

Piping loads did not have any effect on the benchmark results; therefore, the procedures detailed above are also applicable for the addition of piping loads.

Limit analysis or plastic analysis do not predict buckling phenomena (elastic-plastic instability), which require specific analyses. Buckling phenomena often occur with large changes of the overall shape, centred on compressive regions of the structure.

Nevertheless, a plastic instability load is also often associated with large changes of overall shape. These loads can normally be captured by the large displacement theory embodied in a plastic analysis but will not be captured by a limit analysis. As a consequence, if the instability is mainly due to shape modifications which accelerate plasticisation, limit analyses should be used with caution to predict collapse.

3.2.3 Plastic instability recommendations

The following best practices recommendations can therefore be made:

- The limit load method, with an appropriate flow stress, can be used to assess plastic instability.
- The true stress-strain curve should be used for plastic analysis with large displacements/strains, which gives the realistic behaviour of the material.
- The plastic instability load can be assessed by an elastic-plastic calculation: plastic instability is detected by numerical divergence.
- The local location of the maximum strain can be taken to determine the collapse load. It should be noted that this is geometry and mesh dependent and has not been codified.

3.3 Differences in the approaches for 2D & 3D models

As described in Part 2b (2), and previously in Section 2.1.1, higher and more realistic limit loads can be obtained if the geometry is modelled in 3D. Analysts typically prefer to work with a 2D model however to reduce the analysis time. A 2D axisymmetric model, if chosen for the analysis, should replicate the 3D model. As seen in the report, the limit load value increases with the 3D model; this is due to the inherent additional conservativeness built into the 2D model. Analysts should therefore carefully create the 2D axisymmetric model to reduce the risk of error. A linear elastic analysis can then be performed to compare the 2D and 3D results although this might be time-consuming and may not yield valuable results.

3.4 Effects of element types and element sizes

In finite element analysis, the mesh density is a critical issue that has a significant impact on the accuracy of the finite element models and directly determines their complexity level. Four node quad elements should be used for a 2D axisymmetric model, while eight node brick elements (hex) should be used for 3D models if the software options allow. If the geometry is complex, tria and tetra mesh can be used for the FE model. The element density should be increased in

locations that feature geometric discontinuities. During the discretization of a 3D model, a minimum of four elements should be captured along the thickness, since the stress linearization results may vary depending on the number of elements captured along this thickness.

3.5 Interpretation of results

The analysts are responsible for interpretation of the results after completion of the analysis. Post processing of results must be performed for regions of geometric discontinuity. The aforementioned points have a significant impact on the results as shown in previous parts of this series of reports (1) (2). Differences arise from the various codes of practice followed by participants and their in-house requirements. It is therefore recommended that a single standard operating procedure should be developed for limit load analyses, which would outline an approach to post-processing based upon the sound engineering judgement required for dealing with the origin of divergence and the particular zones to be characterized.

4. Elastic fatigue analysis recommendations

Fatigue analysis examines the weakening of a material as a result of being subjected to cyclical mechanical and/or thermal loads. Two types of fatigue exist: elastic fatigue and plastic fatigue. The former is the result of primarily low elastic stress applied over a high number of cycles (>10^4) while the latter occurs after fewer cycles in which there is significant plasticity.

This section presents the steps required for a linear elastic fatigue calculation along with recommendations associated with the undertaking of each step. Plastic fatigue analysis is covered in Section 0 of this report.

It should be noted that this section refers to both Section III, Appendix XIII of the ASME BPVC (6), and RCC-M (4). The recommendations are intended to be generally applicable to other recognized nuclear codes and standards. It should be noted that this section does not present a complete interpretation of ASME BPVC Section III and RCC-M fatigue analysis requirements.

4.1 Overview of elastic fatigue methodology

4.1.1 Basic concepts

The common approach to fatigue in mechanical design codes relies on the use of elastically calculated stresses. Non-linear material behaviours due to plasticity effects are accounted for using plasticity correction (K_e) factors. The elastic methodology allows for the linear superposition of stresses arising from various origins, such as those due to internal pressure, thermal gradients, and dynamic effects. In codified elastic fatigue analysis, a distinction is drawn between constant stresses and those that vary with time. Design codes such as ASME BPVC Section III and RCC-M do not directly consider mean stresses, whose effect is already accounted for in the design fatigue curves. Therefore, static stresses such as deadweight and residual stresses are not included in elastic fatigue analysis, as they do not vary with time and so cannot influence the elastic stress range.

For simplicity, stresses in linear elastic fatigue analysis can generally be categorized into two types:

- Stresses arising from transient mechanical loads, including internal pressure, piping moment/torsion, and dynamic loads. These are sometimes termed mechanical stresses.
- Stresses arising from the non-uniform distribution of temperature in the component. These are termed thermal stresses and are caused by variations in the coolant temperature which is in contact with the internal surface of the component following changes in the plant power state. The thermal stresses evolve based on variations in the axial and radial thermal gradients that exist in the component.

Generally, the contributions of both categories of stresses must be determined independently. This is typically achieved by undertaking separate finite element analysis (FEA) of the different loading conditions experienced by the component in question. The independent contributions of time-varying mechanical and thermal stresses may then be superimposed to determine the total stresses for fatigue analysis. However, continuum FEA stresses are not directly applicable to the elastic fatigue analysis approach of most codes and standards. The elastic FEA stresses must first be manipulated or ‘post-processed’ to obtain the necessary quantities required in the code. This process can have a significant impact on the results of ‘downstream’ fatigue calculations.

The specifics of the calculations and principal considerations are discussed in the sections below.

4.2 Post-processing of finite element stresses

The objective of the finite element post-processing operation is to obtain the stress-time history of the stress categories required for fatigue analysis. The six unique components of the Cauchy stress tensor are required. At a minimum, the stresses required are the primary plus secondary (linearized) stresses and the primary plus secondary plus peak (total) stresses. These are used later in the cycle counting procedure to determine the primary plus secondary stress intensity range (S_n), and primary plus secondary plus peak stress intensity range (S_p).

4.2.1 Consideration of mesh size

The selection of an appropriate finite element mesh is the first important consideration for any fatigue analysis problem. In pressure vessels and piping components, fatigue crack initiation normally occurs on the internal surface. Thus, capturing accurately the surface peak stresses arising due to mechanical and thermal load fluctuations is of paramount importance. This is due to the high non-linearity of the design fatigue curve in the low-cycle regime, where even an inaccuracy in capturing the stress amplitude can result in a rather dramatic effect on the calculated fatigue usage. Accordingly, the mesh refinement should be prioritized near the internal surface of the component.

The level of mesh refinement required will often be dictated by the characteristics of the thermal transients experienced by the component. Factors such as the heat transfer coefficient (HTC), the thermal ramp rate, and thermal resistance of the section under assessment are all significant. Benchmark 2 of Part 2a (1) was specifically selected to explore these factors and different analyst choices for mesh refinement.

Benchmark 2 placed a high demand on the level of mesh refinement due to the characteristics of Transient 2 (T2), wherein the nozzle experiences a very sharp 150°C thermal shock in one second. An infinite HTC between the nozzle and contacting fluid was also specified, essentially resulting in a step-change in the metal surface temperature. Accordingly, the selection of an appropriate mesh discretization near the inner surface was an influential consideration by participants for this problem. Participants adopted a variety approaches for mesh selection, the most common of which was to incrementally refine the mesh until the maximum stress intensity on the internal surface converged to within a given tolerance (*e.g.*, 1-2%).

Another practical option to establish an appropriate mesh size is to utilize the analytical thermal stress solution for the geometry in question. These solutions assume that the thermal and mechanical properties of the material are temperature independent. In the case of Benchmark 2, two locations situated in the main coolant line (S20) and branch pipe (S29) are representative of a thick-walled cylinder. Therefore, the analytical solution derived for a flat plate or pipe can be used at these locations as a close approximation. The element size on the inner surface may then be adjusted accordingly to match closely the surface stresses obtained from the analytical solution. The analytical solution for a plate subjected to an arbitrary fluid temperature change in contact with its inner surface, and an adiabatic condition on its outer surface, has been extensively documented (8). One participant adopted this approach to perform a mesh optimization study for Transient 2, considering element thicknesses, e, of 0.5mm, 1mm, and 1.65 mm on the internal surface layers, with the goal of matching closely the analytical circumferential

(hoop) stress history. Due to the specification of an infinite HTC, it is not possible to match exactly the analytical solution without excessive computational cost; the best that can be expected in such situations is to achieve an acceptable compromise between accuracy and solution time. Some slight differences would also be expected since ultimately the analytical solution is only a close approximation of the true structural behaviour in this case. Figure 3 and Figure 4 show a comparison between the analytical and FEA solutions respectively for assessment locations S20 and S29 obtained by the participant at the peak of the Transient 2 cold shock period (50 to 52 seconds) for the different element inner layer thicknesses considered. Table 1 shows the comparison of the peak thermal hoop stresses calculated in each case. The results suggest that an inner element thickness of 1 mm is sufficient to capture the peak thermal stresses with reasonable accuracy and without excessive computational cost. Analytical solutions therefore serve as a useful tool to assist in assessing the validity of FEA computations and it is recommended that they be used where possible.

Where practical, the choice of mesh should also be evaluated with respect to its effect on the final input values used in code assessments and potential 'knock-on effects' in the downstream fatigue calculations. As shown by Figure 5, the effect of inner surface mesh refinement on S_p is likely to be more significant for more rapid thermal shock transients. In the case of Benchmark 2, little difference is observed between the various mesh sizes for Transient 1, whilst greater differences can arise for Transient 2, where the thermal shock is much sharper.

It is therefore recommended that the mesh size adopted by analysts for a specific fatigue problem should be established considering the design transient with the most severe thermal ramp rate and HTCs. As shown by Figure 6, S_n tends to be relatively insensitive to mesh density, and therefore the effect on S_p is of greatest importance.

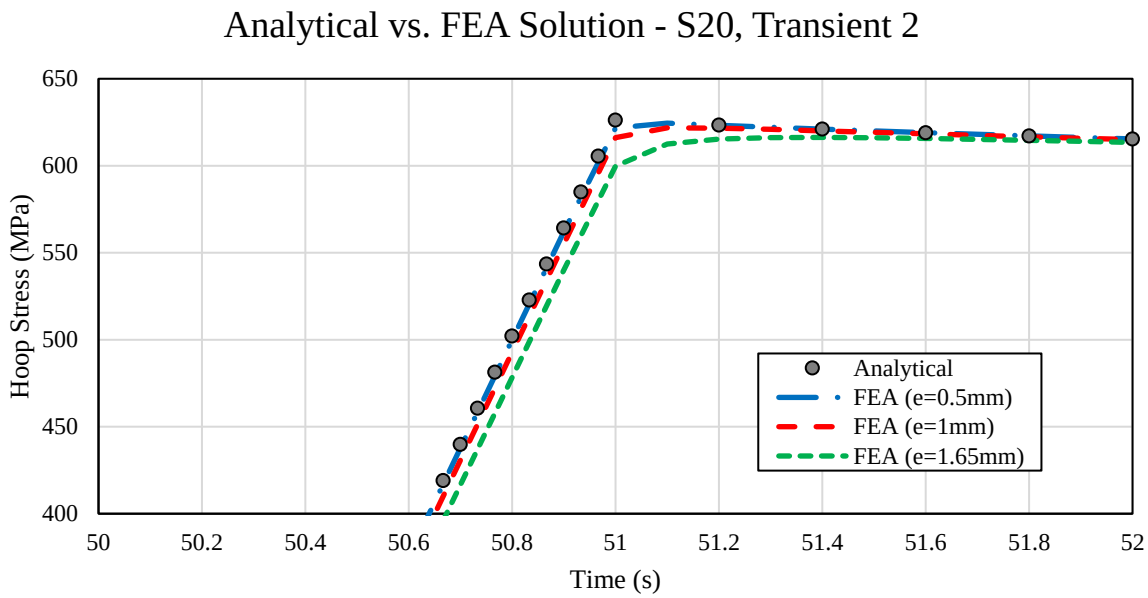

Figure 3. Analytical vs FEA solution for S20, Transient 2

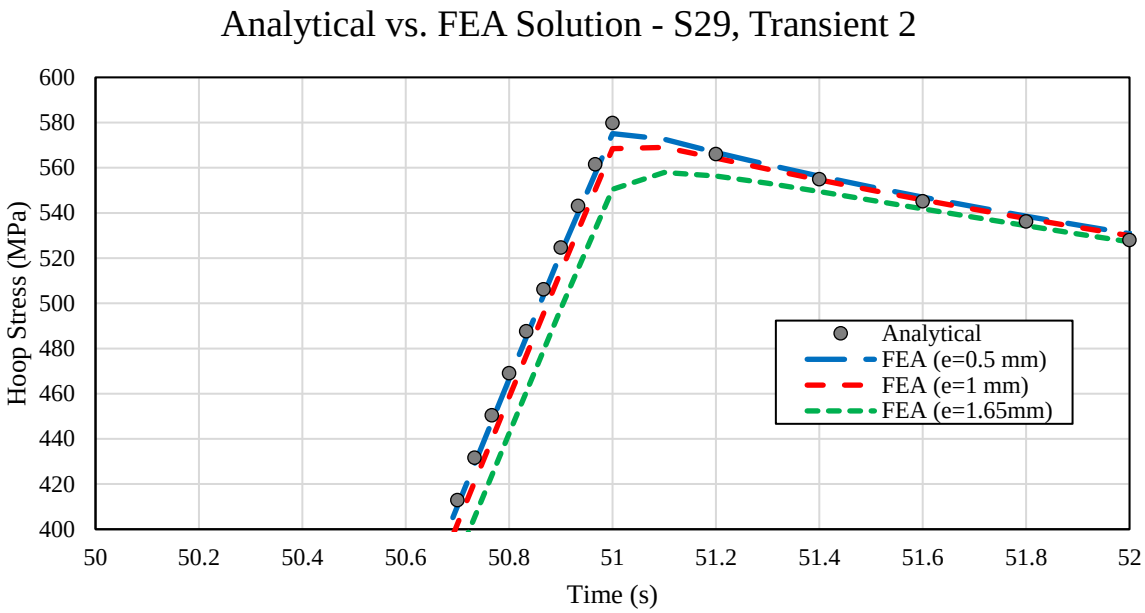

Figure 4. Analytical vs FEA solution for S29, Transient 2

Table 1. Analytical vs FEA comparison of peak thermal hoop stresses, Transient 2

	Assessment Location	Maximum Hoop Stress (MPa)			
		Analytical	FEA (e=1.65mm)	FEA (e=1.0mm)	FEA (e=0.5mm)
Inner Surface	S29	579.82	557.92 [-3.78%]	569.01 [-1.86%]	575.11 [-0.81%]
	S20	626.14	616.29 [-1.57%]	621.79 [-0.70%]	624.50 [-0.26%]

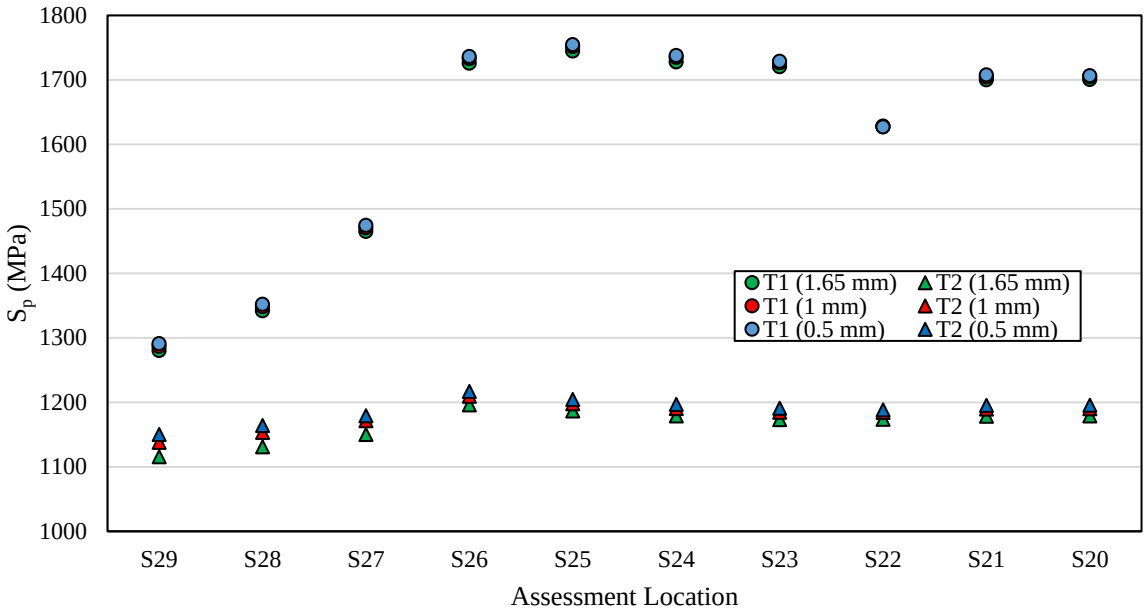

Figure 5. Effect of mesh refinement on S_p

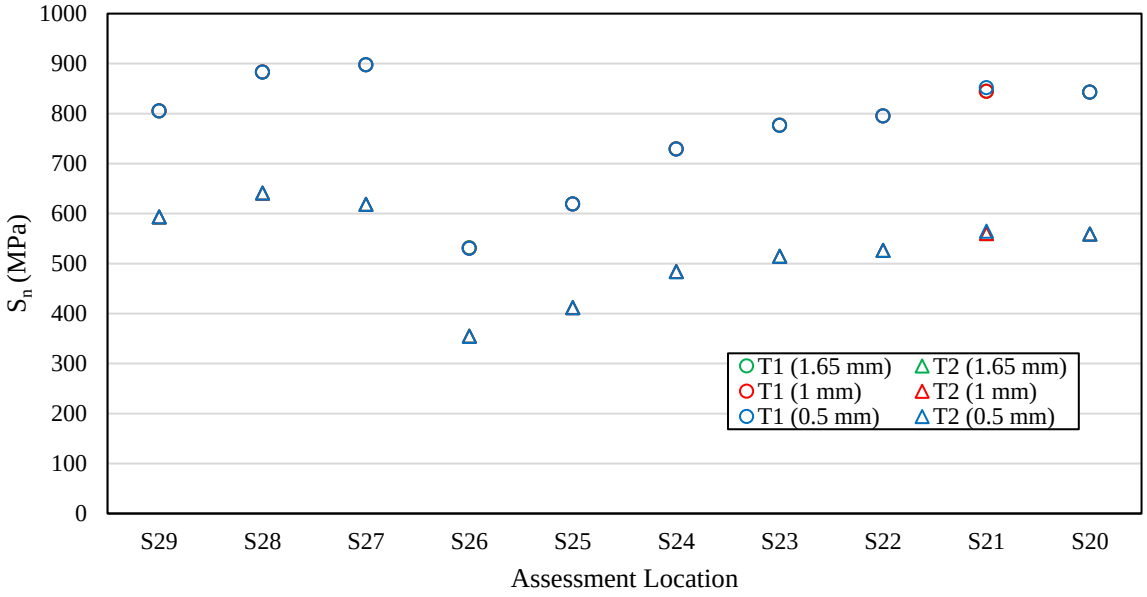

Figure 6. Effect of mesh refinement on S_n

4.2.2 Stress classification lines

In performing codified elastic fatigue analysis, the fatigue usage is evaluated at discrete locations, known as stress classification lines (SCLs). The SCL represents a straight line spanning the section thickness of a pressure vessel or piping component. The inner and outer points of the SCL are situated on the internal and external surface of the component and it is these points that must be assessed. Generally, fatigue tends to be most severe on the internal surface and thus the interior point of the SCL is of much greater significance.

The orientation of the SCL is very important. Normally, SCLs will be positioned perpendicular to the inner and outer surfaces and therefore normal to the mid-plane through-thickness. However,

there are some situations where this is not possible, as it would not capture the location of highest stresses. Recommendations for dealing with these situations are provided in ASME BPVC Section VIII Division 2, Annex 5-A, Article 5-A.3 (9) and RCC-MRx RB 3224.11 (10). In these situations, care should be taken to ensure that the SCL is oriented perpendicular to the computed stress contours' through-thickness. A good example of this situation is in the crotch region of vessels and piping nozzles, which can often be the fatigue limiting location.

In the assessment of typical components, many SCLs will generally be required to cover the main regions of high stresses, local structural discontinuities, and material discontinuities. If geometric discontinuities are not represented in sufficient detail by the FE model, then the application of an appropriate stress concentration factor (SCF) or fatigue strength reduction factor (FSRF) is necessary. Care must be taken in the assessment of material discontinuities in FEA, in particular dissimilar metal welds since thermal mismatch can induce a sharp discontinuity in the stress field. The recommendation here is to take lines either side of the interface but avoiding the singularity. Stress ranges along the length tend to be less sensitive to mesh density and sensible locations for assessment can be determined by plotting the stress variation at the surface across the interface.

The most important function of the SCL is to allow for calculation of stress resultants across the section using continuum FEA stresses. This is the objective of stress linearization.

4.2.3 Linearization of stresses

Stress linearization (see also Section 2.2.3) is one possible methodology adapted for use in FEA software, which can be used to extract membrane and bending stress resultants at the SCL locations. Here, the term 'total stress' is used to refer to the continuum FEA stress and is denoted by σ_{ij}.

Each of the six-tensor stress non-linear distributions has an equivalent membrane stress distribution, $\sigma_{ij,m}$, which may be determined by Equation 7 below.

$$\sigma_{ij,m} = \frac{1}{\mathrm{e}} \int_0^e \sigma_{ij}(x)\, dx$$

Equation 7

Membrane stress is defined as the average stress along the SCL and by definition is constant through-thickness. Similarly, to membrane stress, each of the six-tensor stress non-linear distributions has an equivalent 'bending' stress distribution, $\sigma_{ij,b}$, and is determined from:

$$\sigma_{ij,b} = \frac{6}{\mathrm{e}^2} \int_0^e \sigma_{ij} \left(\frac{e}{2} - x\right)\, dx$$

Equation 8

Bending stress is the part of the stress distribution that varies linearly across the SCL and has the greatest magnitude on one of the surfaces (or 'outer-fibre'). A key characteristic of the bending stress is that it integrates to net zero force and produces the same net bending moment as the total stress distribution across the SCL. Peak stresses are defined as the difference between the total stress, considering any FSRFs and SCFs where necessary, and the sum of the membrane and bending stress contributions.

$$\sigma_{ij,F}(\mathrm{x})\big|_{x=0} = \sigma_{ij}(\mathrm{x})\big|_{x=0} - (\sigma_{ij,m} + \sigma_{ij,b})$$

Equation 9

$$\sigma_{ij,F}(\mathrm{x})\big|_{x=t} = \sigma_{ij}(\mathrm{x})\big|_{x=t} - (\sigma_{ij,m} - \sigma_{ij,b})$$

Equation 10

In this report, the primary plus secondary stresses (P+Q) are assumed equal to the sum of the membrane plus bending stresses:

$$\sigma_{ij,P+Q} = \sigma_{ij,m+b} = \sigma_{ij,m} + \sigma_{ij,b}$$

Equation 11

It is crucially important that the stresses be first transformed from the default global coordinate system defined in the FEA software, to the local coordinates associated with the SCL under assessment, prior to performing stress linearization. In this report, the following coordinate conventions are used: the local x-direction is parallel to the SCL (radial); the local y-direction is tangential to the SCL (axial), and the local z-direction is in the circumferential plane (meridional/hoop).

One circumstance that can arise is the possibility of the primary plus secondary stress time history being out-of-phase (lagging) with the total stress time history. This is because the primary plus secondary stress is highly dependent on the section thickness and can have a much slower stress response than that of the total stresses. This can be especially significant for thick-walled components.

To illustrate this, consider the case of a pipe of internal radius of 350 mm and thickness varying from 10 mm to 120 mm subjected to a sharp thermal shock. In this example, the linearization was performed considering 200 equally spaced points through-thickness. Figure 7 shows the total and P+Q hoop stress response for two different thicknesses of 30 mm and 120 mm. As can be seen, for the 30 mm pipe thickness, the total and P+Q response vary in-phase. On the other hand, for the 120 mm thick pipe, the P+Q stress significantly lags that of the total stress, and only achieves its peak around 200 seconds after the initial thermal shock. At the beginning of the shock, the peak stress is high and the linearized stress is low, as the temperature homogenizes through the wall, the linearized stress will increase. Whilst this represents an extreme example, it is not unusual to observe some lag in the P+Q stress in realistic cases, which can have an impact when it comes to cycle counting. Therefore, there are two recommendations here:

The first recommendation is that stress linearization should be performed at every time-step in the FE stress history, and not just at the times at which the total stresses are known to be extreme. The full time history of the P+Q stress should always be generated unless it is known with certainty that the total and P+Q stress histories are very closely aligned (*e.g.*, for thin-walled piping subjected to less sharp thermal transients).

The second recommendation relates to the time-step discretization adopted by analysts. In this case, it is important that the time-steps used in both the thermal and structural FEA are adequately refined both during the loading event, to capture the extreme in the total stress, and for some period after the loading event, to capture the extreme in the P+Q stress. This requires an element of analyst judgement on a case-by-case basis. The time-step size generally does not need to be as refined as that adopted for the initial loading event, so long as it is small enough to capture approximately the extreme in the P+Q stress.

The choice of which stress components to linearize can also potentially influence the magnitude of the P+Q principal stresses, and consequently can affect the calculated S_n in downstream fatigue calculations. Welding Research Council (WRC) Bulletin 429 (11) discusses four options for calculation of linearized principal stresses:

1. Membrane plus bending for all six stress tensor components.
   - Default route in most linearization tools built into FEA software.
   - 'Bending' is not defined for radial and shear components.
2. Membrane plus bending for the direct stress components; membrane only for shear.
   - 'Bending' is not defined for the radial component.
3. Membrane plus bending for hoop and axial components; membrane for other components.
   - Bending is computed only for components with valid bending.
   - Recommended in WRC-429 since it best follows guidance within ASME BPVC Section III.
   - Adopted within ASME BPVC Section VIII-2 Div. 2, Annex 5-A.
4. Membrane plus bending for direct stress components; FE (total) stresses for shear.
   - Conservative since total shear stresses are used as bending.

Generally, linearization of all stress components tends to be most prevalent within industry since this is often the default option utilised by FE-based linearization tools. Out of the options above, only options 1 and 3 are relevant for plane un-notched sections in vessels and piping where the SCL is oriented perpendicular to the mid-plane through-thickness; options 2 and 4 will have no impact in this case since shear is negligible.

The influence of the linearization technique on S_n was investigated for the auxiliary piping nozzle described in Benchmark 2 of (1). The variation of S_n calculated at the inner and outer surfaces are shown in Figure 8 and Figure 9, respectively. The solid markers denoted the values calculated for Transient 1, whilst the open marker denoted the values calculated for Transient 2. As can be seen, there is not a significant difference between the different methods for the branch pipe (S27-29), crotch corner (S22), and MCL run pipe (S20-21). In the case of the nozzle region (S23-26), the WRC-429/ASME VIII-2 method gives somewhat more conservative results than linearizing all stress components.

The choice of linearization method only becomes significant in situations where the radial through-wall stresses are non-negligible, which is generally limited to thick-walled piping and vessels or conditions where a large axial thermal gradient develops. In such situations, the radial P+Q stress, $\sigma_{x,P+Q}$, is lower when using the WRC-429/ASME VIII-2 method due to neglecting the fictitious bending contribution. This algebraic difference between the principal P+Q stresses is therefore larger for WRC-429/ASME VIII-2, resulting in a higher value of S_n. The difference in S_n is however relatively minor (<10%).

Table 2 shows the difference in the ASME III CUFs calculated for Benchmark 2.0 based on both options. As can be seen, WRC-429/ASME VIII-2 predicts higher CUFs in the nozzle region up to a maximum of 45%. Nevertheless, the maximum CUFs are equal and in the same location. The main situation where it may be expected to have some impact is in the case where S_n is close to

the $3S_m$ limit, and therefore the choice of linearization technique could mean the difference between needing to apply a plasticity correction factor (K_e) or not. In such situations, analysts may wish to perform sensitivity studies to examine the choice of linearization technique on the results.

In the case of plane un-notched sections, the choice of linearization technique adopted is not considered to be an issue for fatigue analysis in more realistic cases. In the case of sharper notches, or more significant shear loading, the choice of linearization technique may be expected to show a greater difference. However, high shear stresses are relatively rare in pressure vessels and piping components since they normally only arise due to non-proportional loading. Since fatigue crack nucleation usually occurs on the internal surface, this essentially fixes one of the three principal axes. The other two axes can only rotate in the presence of time-varying, out-of-plane shear loading, which can only feasibly occur in nozzles subjected to high torsional loads induced by the motions of an attached piping system. This situation is rare in practice and is usually a consequence of poor design.

Therefore, based on the above observations, it is concluded that the choice of linearization technique may be significant in very specific situations. Whilst the WRC-429/ASME VIII-2 is technically the 'correct' method based on shell discontinuity theory and does appear to produce more conservative results in some situations, it is important to recognize that this may not be appropriate for thick-walled components. Therefore, the following recommendation is proposed:

The third recommendation is that the calculation of membrane and bending stress resultants should be performed for all six unique components of stress as a 'default' approach for fatigue analysis problems. This approach is considered to have the widest range of applicability and is the most practical to implement within existing software.

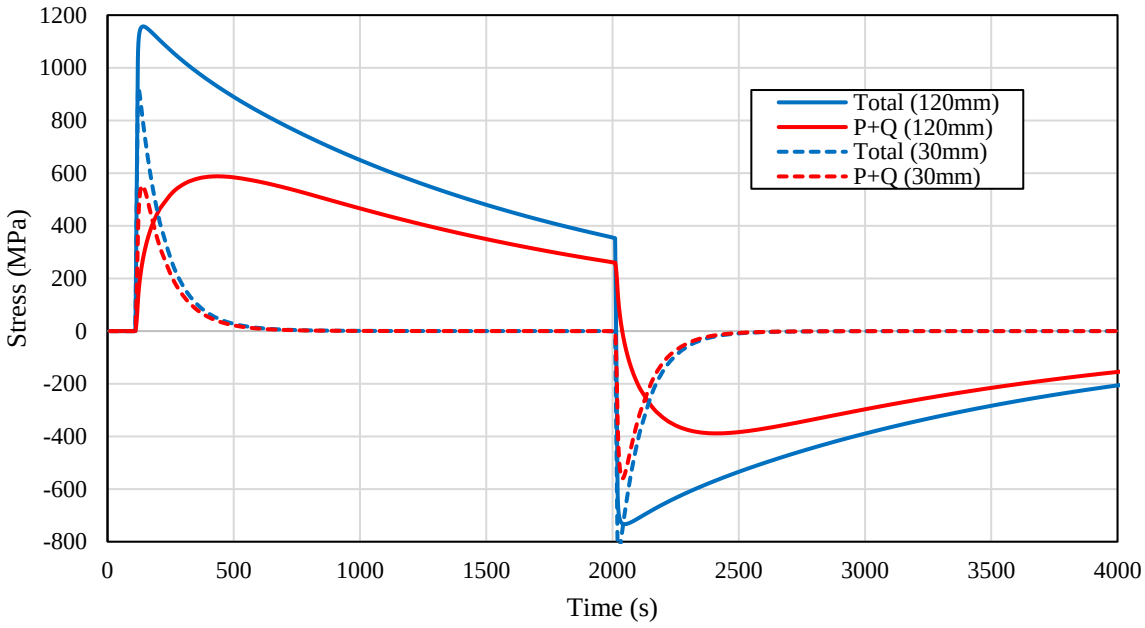

Figure 7. Total and P+Q hoop stress response for simple pipe

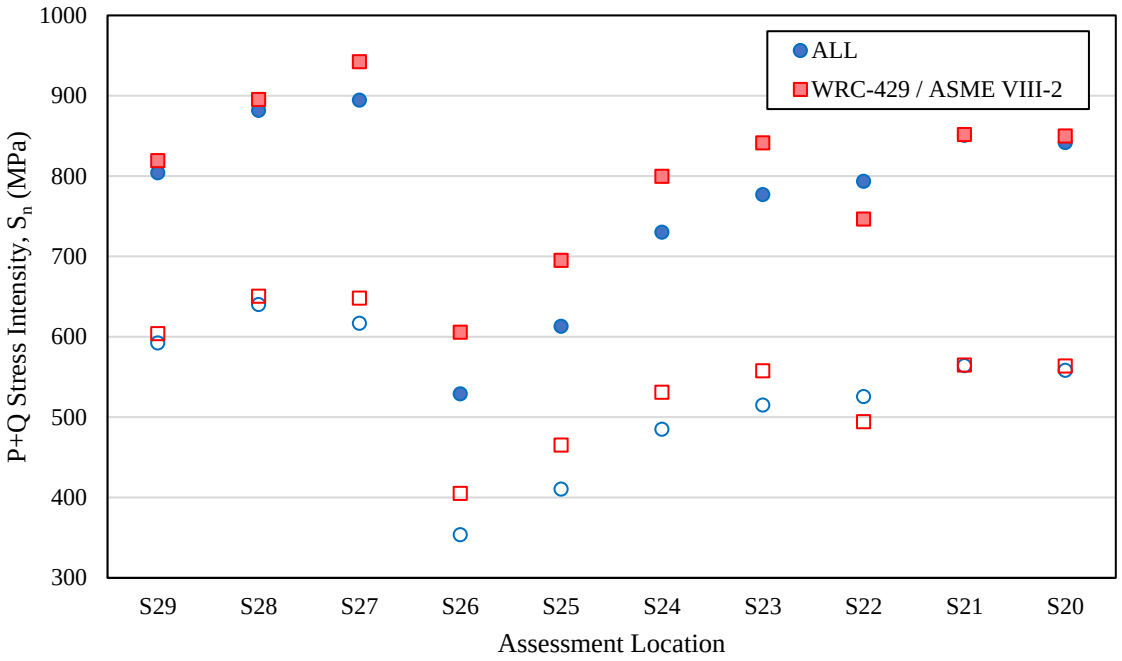

Figure 8. Variation of S_n at inside surface according to linearization method

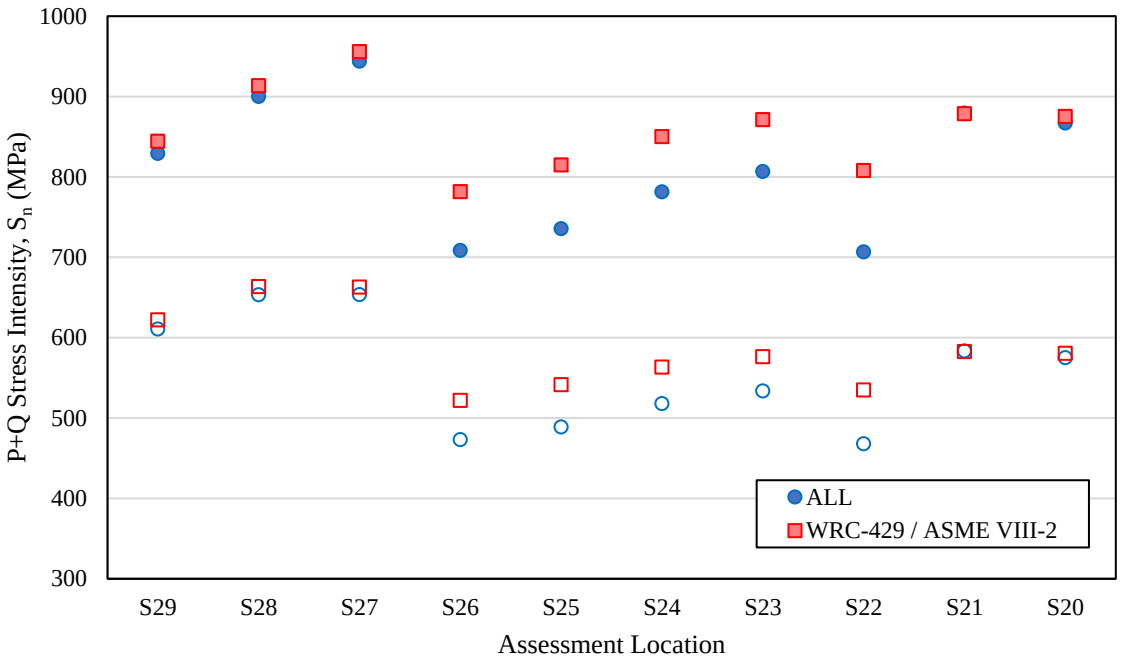

Figure 9. Variation of S_n at outside surface according to linearization method

Table 2. Summary of ASME III CUFs depending on stress linearization technique.

	Assessment Location	Cumulative Usage Factor		
		All	WRC-429	Diff (%)
Inner Surface	S29	11.083	11.083	0.00%
	S28	11.517	11.517	0.00%
	S27	12.190	12.190	0.00%
	S26	4.763	6.761	29.55%
	S25	7.053	9.888	28.67%
	S24	10.911	13.360	18.33%
	S23	12.811	13.222	3.10%
	S22	12.900	11.123	-15.97%
	S21	13.244	13.244	0.00%
	S20	13.254	13.254	0.00%
	Assessment Location	Cumulative Usage Factor		
		All	WRC-429	Diff (%)
Outer Surface	S29	0.747	0.747	0.00%
	S28	1.080	1.080	0.00%
	S27	1.270	1.270	0.00%
	S26	0.113	0.163	30.52%
	S25	0.146	0.184	20.50%
	S24	0.276	0.285	3.07%
	S23	0.365	0.365	0.00%
	S22	0.248	0.367	32.49%
	S21	0.814	0.814	0.00%
	S20	0.771	0.771	0.00%

4.3 Cycle counting and load combinations

The objective of cycle counting is to identify the time points within one or more transient stress-time histories that constitute stress reversals, and to combine these time-points in such a way to produce well-defined stress cycles. The background and best practice recommendations outlined in this section are discussed in the context of an ASME BPVC Section III Appendix XIII-3500 fatigue evaluation. However, some important observations relating specifically to RCC-M B 3200 (12) are also highlighted.

4.3.1 Background

ASME BPVC Section III Appendix XIII-1300(ag) defines a stress cycle as:

> *A condition in which the alternating stress difference goes from an initial value through an algebraic maximum value and an algebraic minimum value and then returns to the initial value. A single service cycle may involve one or more stress cycles*.

In this statement, the phrase 'service cycle' is interchangeably referred to as an event or transient.

Various methodologies for identifying stress cycles have been proposed within the technical literature, for application to both uniaxial and multiaxial stress histories. In most design codes, simplified uniaxial cycle counting methods are common, where the identification of stress cycles is normally performed on the time history of the signed 'equivalent' stress, that is, either Tresca or von Mises stress intensities. The simplest approach is that of extreme value pairing (EVP), also known as 'peak-to-peak' (PTP) counting, and is the methodology adopted within ASME BPVC Section III. The procedure involves identifying the relative peaks and valleys in the uniaxial stress-time history and pairing each peak and valley in order of decreasing stress range, eliminating each pair after they are counted. After all pairs are accounted for, the cycle counting procedure is complete. The output of EVP is a list of stress ranges in order of highest-to-lowest.

An illustration of EVP is provided in Figure 10 and Figure 11. Figure 10 shows an arbitrary uniaxial reversal history, which may be identified from the FEA stress-time history for each of the transients under consideration. Figure 11 illustrates the steps followed by EVP. In this case, the stress-time history is reordered based on absolute magnitude whilst retaining the sign convention (though this is not a strict requirement of EVP); identifying the relevant stress ranges is then trivial. The highest stress range is identified by the two points marked with circles, the second highest with triangles, the third highest with squares, and so on. This pairing of extreme points in the loading history to produce corresponding ranges continues until no more reversal loci remain.

One of the benefits of EVP is that it need not necessarily be applied to an actual loading history obtained in sequence. The order of events does not affect the output obtained from EVP and thus the stress history may be ordered in or out of sequence with that observed under representative plant transient conditions. The hoop stress history shown in Figure 12 represents example of an unordered sequence of design transients, each with an estimated frequency of occurrence, which are expected to arise during the lifetime of a component. As the order in which plant transients are likely to occur cannot be known with certainty especially for Service Level B transients, the EVP is often the most appropriate option for design fatigue analysis.

In performing a fatigue assessment to ASME BPVC Section III, the EVP is applied in accordance with ASME III Appendix XIII-2420 and XIII-3520 (e). In ASME III, the critical time-points across all transients where the stress achieves a peak or valley are directly combined. The calculation of the alternating stress intensity for each cycle can then proceed.

The necessary steps are summarized algorithmically as follows:

1) Determine the total (including peak) elastic principal stress history for the individual, or combination of loading events.
2) Identify points in the loading history where conditions are known to be extreme (*i.e.*, reversal loci) and delete all other intermediate points.
3) Initialize the number of cycles to zero, $M = 0$.

4) Identify the stress states at two time points, ${}^{m}t$ and ${}^{n}t$, that produce the maximum Tresca stress intensity range, $\Delta\sigma_I$.

$$\Delta\sigma_I = Max\left[abs({}^{mn}\Delta\sigma_1 - {}^{mn}\Delta\sigma_2), abs({}^{mn}\Delta\sigma_2 - {}^{mn}\Delta\sigma_3), abs({}^{mn}\Delta\sigma_3 - {}^{mn}\Delta\sigma_1)\right]$$

Equation 12

Where

$${}^{mn}\Delta\sigma_i = {}^{n}\sigma_i - {}^{m}\sigma_i,\ for\ i = 1,2,3;\ \ {}^{m}\sigma_i = \sigma_i({}^{m}t)\ and\ {}^{n}\sigma_i = \sigma_i({}^{n}t)$$

5) Increment the number of cycles by one, $M = M + 1$. Record each pair of time points for the M^{th} cycle, ${}^{m}t$ and ${}^{n}t$, and their associated number of repetitions, ${}^{m}n$ and ${}^{n}n$. Set the stress range of the M^{th} cycle to $\Delta\sigma_M = \Delta\sigma_I$. Set the number of repetitions of the M^{th} cycle to $\min\left[{}^{m}n, {}^{n}n\right]$.

6) Determine the number of cycle repetitions in accordance with ASME BPVC Section III NB-3222.4(e)(5).
   - If ${}^{m}n < {}^{n}n$, delete ${}^{m}t$ from the loading history and reduce the number of repetitions at ${}^{n}t$ by ${}^{m}n$.
   - If ${}^{m}n > {}^{n}n$, delete ${}^{n}t$ from the loading history and reduce the number of repetitions at ${}^{m}t$ by ${}^{n}n$.
   - If ${}^{m}n = {}^{n}n$, delete both ${}^{m}t$ and ${}^{n}t$ from the loading history.

7) Repeat steps 3 through 5 until all reversal points in the loading history are eliminated. The EVP cycle counting procedure is complete. The final list of M cycles is obtained with stress intensity ranges given by $\Delta\sigma_k, k = 1, \ldots, M$.

The output of the EVP is a vector containing the stress intensity ranges ('cycles'), the time points defining the 'peak' and 'valley' stress states, and an associated number of repetitions for each cycle. The cumulative usage factor (CUF) is then evaluated by performing the following steps for each identified cycle: $k \leq M$.

1) Obtain the total stress tensor at the start and end time points of the k^{th} cycle, ${}^{m}\sigma_{ij,k}$ and ${}^{n}\sigma_{ij,k}$, and the membrane plus bending stress tensor, ${}^{m}\sigma^{mb}_{ij,k}$ and ${}^{n}\sigma^{mb}_{ij,k}$.

2) Determine the total and membrane plus bending principal stress ranges between the start and end time points of the k^{th} cycle, $\Delta\sigma_{i,k}$ and $\Delta\sigma^{mb}_{i,k}, i = 1,2,3$.

3) Calculate the primary plus secondary plus peak stress intensity range for the k^{th} cycle, $\mathrm{S}_{\mathrm{p,k}}$:

$$S_{p,k} = Max\left[abs(\Delta\sigma_{1,k} - \Delta\sigma_{2,k}), abs(\Delta\sigma_{2,k} - \Delta\sigma_{3,k}), abs(\Delta\sigma_{3,k} - \Delta\sigma_{1,k})\right]$$

Equation 13

4) Calculate the primary plus secondary stress intensity range for the k^{th} cycle, $\mathrm{S}_{\mathrm{n,k}}$:

$$S_{n,k} = Max\left[abs(\Delta\sigma^{mb}_{1,k} - \Delta\sigma^{mb}_{2,k}), abs(\Delta\sigma^{mb}_{2,k} - \Delta\sigma^{mb}_{3,k}), abs(\Delta\sigma^{mb}_{3,k} - \Delta\sigma^{mb}_{1,k})\right]$$

Equation 14

5) Compute the plasticity correction factor, K_e, in accordance with Appendix XIII-3450(b):

$$K_{e,k} = \begin{cases} 1.0 & if\ S_{n,k} \leq 3S_m \\ 1.0 + \dfrac{1-n}{n(m-1)}\left(\dfrac{S_n}{3S_m} - 1\right) & if\ 3S_m < S_{n,k} \leq 3mS_m \\ \dfrac{1}{n} & if\ S_{n,k} \geq 3mS_m \end{cases}$$

Equation 15

6) Calculate the elastic modulus adjustment factor for the k^{th} cycle, $E_{mod,k}$. $E_{a,k}$ is the representative value of elastic modulus for the k^{th} cycle, whilst E_c is the reference elastic modulus of the design fatigue curve.

$$E_{mod,k} = E_c / E_{a,k}$$

Equation 16

7) Calculate the effective alternating stress amplitude for the k^{th} cycle:

$$S_{alt,k} = \frac{1}{2} S_{p,k} K_{e,k} E_{mod,k}$$

Equation 17

8) Determine the allowable number of cycles, $N_{f,k}$, corresponding to $S_{alt,k}$ computed for the k^{th} cycle using the applicable ASME III Appendix I design fatigue curve.
9) Calculate the partial usage factor (PUF) for the k^{th} cycle where the expected number of repetitions of the k^{th} cycle is denoted n_k:

$$PUF_k = \frac{n_k}{N_{f,k}}$$

Equation 18

10) Calculate the cumulative usage factor (CUF) by linear summation of the PUF obtained for all counted cycles $k = 1, \dots, M$.

$$CUF_k = \sum_{k=1}^{M} PUF_k$$

Equation 19

If the CUF is less than unity, then the location within the component satisfies the fatigue check.

In the basic procedure outlined here, several different routes can be taken depending on interpretation. These can affect the final calculate calculated value of the CUF, sometimes significantly so. These are discussed in the sections that follow.

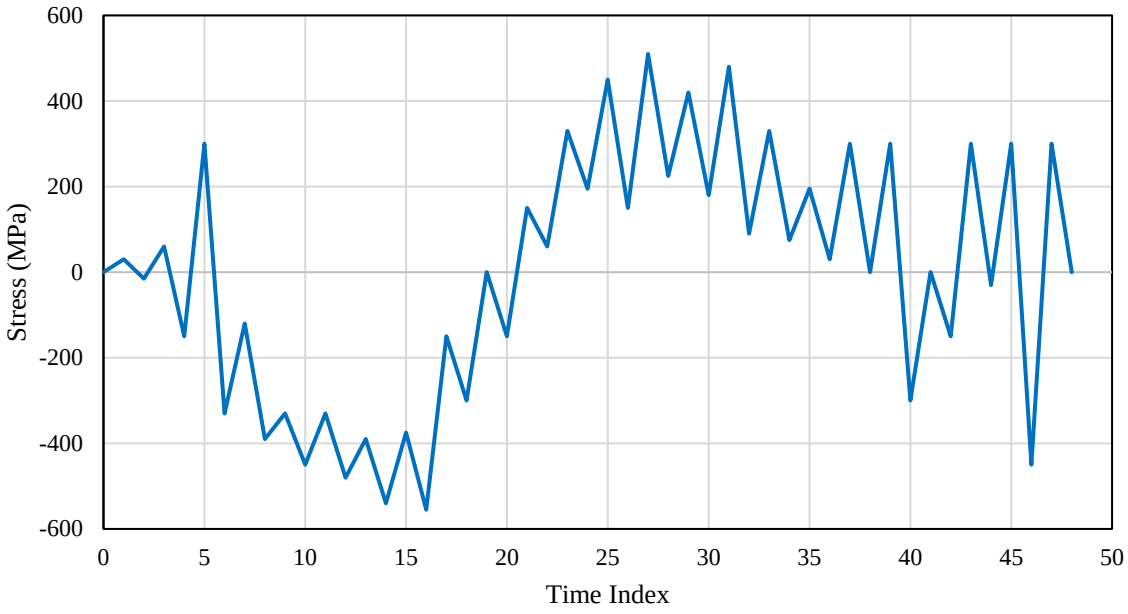

Figure 10. Arbitrary uniaxial reversal history prior to cycle counting

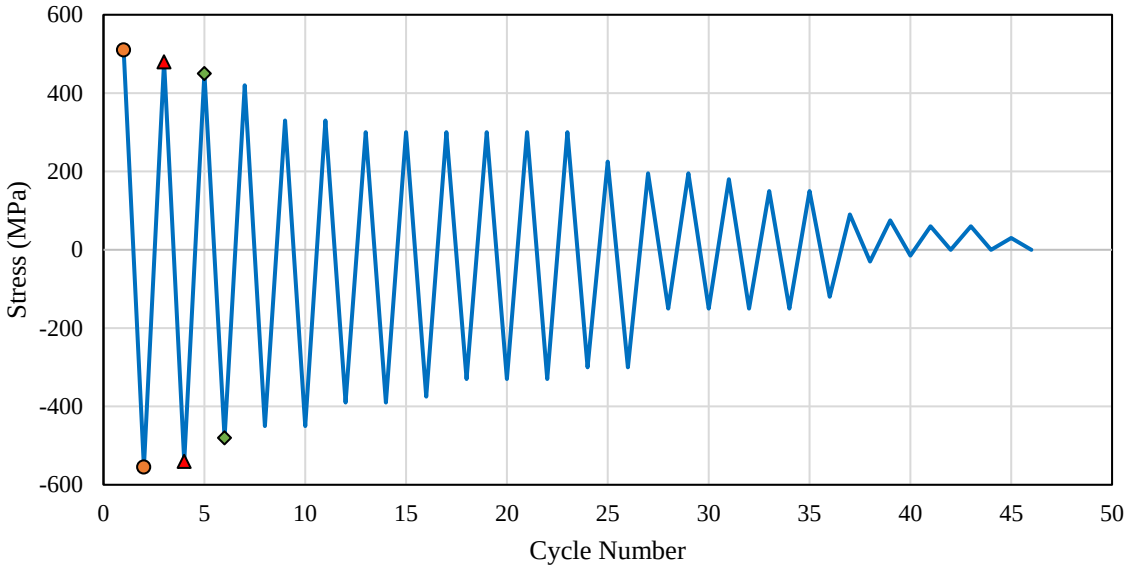

Figure 11. Peak-to-peak cycle counting applied to reversal history of Figure 10

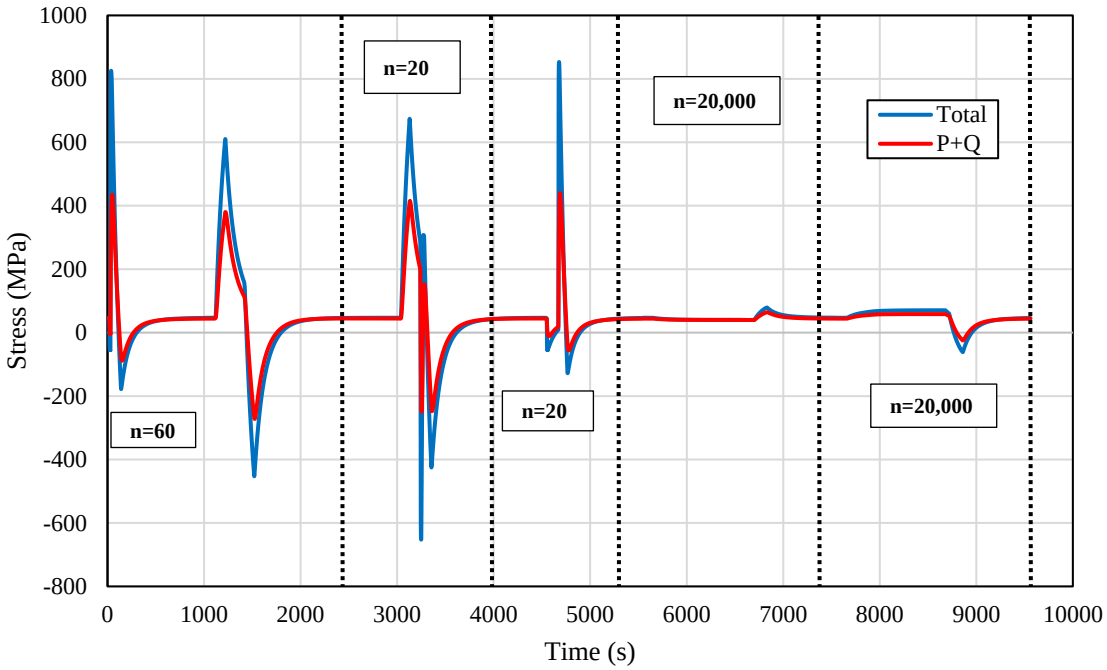

Figure 12. Example of a stress history obtained for an unordered sequence of design transients

4.3.2 Selection of time pairs

The most common analyst judgement is the approach used to calculate S_p and S_n for each cycle. As highlighted in Section 0, the P+Q stresses can vary out-of-phase with the total stress, and therefore the peak and valley respectively forming S_p and S_n do not normally coincide. This is important since the alternating stress is a function of both the K_e and S_p, where K_e is a function of S_n and the design stress intensity, S_m. In ASME Section III, the cycle counting is performed to determine the maximum S_p and does not state as an explicit requirement that S_n need be independently maximized. However, this can obviously have a significant impact on the results since, due to the bounding nature of the ASME BPVC Section III Appendix XIII-3450 K_e, even a modest increase in S_n can produce quite a large plasticity correction.

Three possible options can be taken depending on the degree of conservativeness required.

1) Perform the calculation as described in Section 0, where S_n is calculated based on the time points that maximize S_p.

- For thin sections, this may be acceptable as there will normally be minimal lag between the total and P+Q stresses.
- However, for thicker sections, this will not capture the maximum S_n.
- Since the S_p and S_n both arise due to the same loading event, it is argued to be non-conservative not to account for both in the calculation.

2) Perform the calculation as described in Section 0, but instead independently maximizing S_n by identifying the separate pair of time-points where it is at a peak or valley.

- This option is guaranteed to produce the most conservative value of S_{alt} since it maximizes both S_p and K_e.
- This can be achieved by scanning the $P+Q$ stress-time history in a user-defined window around the time points that form S_p.

3) Perform the calculation as described in Section 0, and determine the single pair of time points which maximizes S_{alt}.

- The rational of this approach is that the maximum S_{alt} for the cycle must be located between the time intervals where S_p and S_n are maximized.
- This approach is likely to produce results that fall between options 1 and 2 in terms of conservatism and has the benefit that only a single pair of time points define the cycle.
- However, a problem with this approach can arise in practice. ASME III considers both surface and sectional plasticity corrections as mutually exclusive, with the former applying for $S_n \leq 3S_m$ and the latter applying for $S_n > 3S_m$. However, for cycles where is S_n close to the $3S_m$ limit, this can produce oscillations in the S_{alt} values from both plasticity corrections turning on and off. It can therefore be difficult in some situations to identify which pair of time points to select using this approach.

To illustrate the potential difference in the results, the calculations associated with options 1 and 2 above were performed for Benchmark 2.0. In the case of option 2, S_n was calculated by scanning the $P+Q$ stress history within a time window of 100 time points either side of the peak-valley points that form S_p. Figure 13 shows the variation in the ASME III Appendix XIII-3450 K_e factor calculated on the inner surface for Transients 1 and 2, depending on the option used to calculate S_n. As can be seen, the K_e factors calculated from option 2 are significantly higher than option 1, as it captures fully the maximum S_n, which lags the maximum S_p. Indeed, option 1 predicts much lower K_e factors in the nozzle and MCL piping where S_p and S_n experience the greatest phase difference. In contrast, when adopting option 2 for calculation of S_n, the maximum K_e factor of 3.33 is predicted at most locations, except for S23-S26 for Transient 2.

Table 3 summarizes the CUFs calculated according to ASME III, depending on the calculation adopted for calculating S_n. The choice of calculation option for S_n can have a very significant impact on the CUFs. When calculating S_n according to option 1, the maximum CUF of 4.750 is predicted to occur at S28 in the branch piping. In contrast, option 2 predicts the maximum CUF of 13.362 to occur at S20 in the MCL piping. On the inner surface, the difference in CUFs calculated using each option is greatest for S23 in the nozzle, which is 12.967 in the case of option 2 compared to 1.491 for option 1, which represents a large increase of 770%. On the outer surface, S_n does not tend to lag S_p as much as for the inner surface and therefore the difference in CUFs between each calculation method is much less significant.

Based on these observations, it is recommended that the S_p and S_n for each counted cycle be determined independently for the calculation of K_e and S_{alt} using option 2 above. This ensures an appropriately conservative result. In determination of S_n, it is important to consider a large enough range around the time points that form S_p, but not so large that it leads to an overlap with other cycles. This can be achieved either by using programming methods or by analyst judgement through manual inspection of the stress histories. It may not necessarily be crucial to capture the maximum S_n for each cycle, so long as this effect is adequately taken into account.

This approach has also been found to be acceptable for use with more complex K_e methods that involve other categories of stress (*e.g.*, Code Case N-779 and Case 17-225) and subtraction of certain stress ranges. For example, Code Case N-779 requires the calculation of local thermal stress range, $S_{p,lt}$, the total stress range less the local thermal stress, $S_{p\text{-}lt}$, and the total stress range less the local thermal and thermal bending stresses, $S_{p\text{-}tb\text{-}lt}$. In this situation, the calculation of the K_e factor should always consider these stress ranges between the time points that form S_n. This ensures that the sum of the membrane, bending, and peak stress ranges will always give the total stress range. Any attempt to combine S_p and S_n based on two different pairs of time points will violate this condition and can lead to erroneous results in the K_e factor calculation using these more complex methods. After the K_e has been calculated based on the maximum range of S_n, it can then be multiplied by the maximum S_p as normal to determine the magnitude of S_{alt}.

(The above is not necessarily an issue for RCC-M where K_e in B3234.6 is to be calculated based on maximization of S_n.)

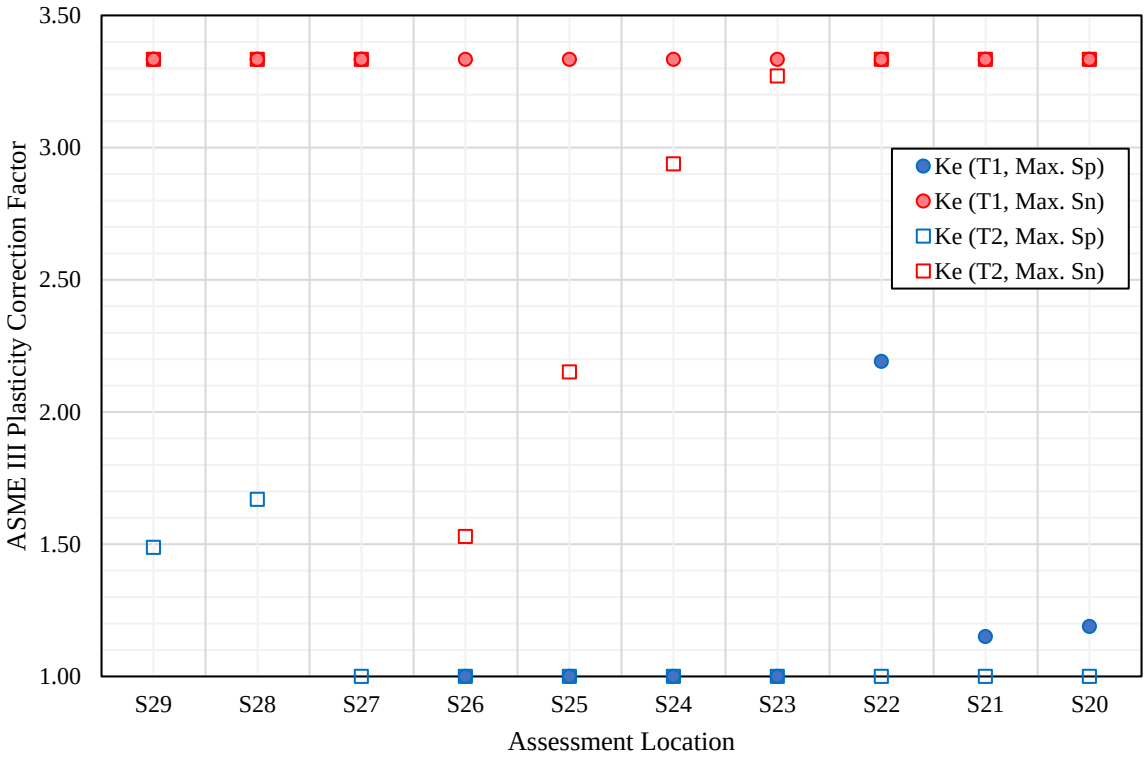

Figure 13. ASME III K_e factors calculated at inner surface according to options 1 and 2

Table 3. Summary of ASME III CUFs depending on S_n time points from options 1 and 2

	Assessment location	Cumulative Usage Factor		
		Option 1	Option 2	Diff (%)
Inner Surface	S29	3.084	11.083	259.34%
	S28	3.793	11.517	203.61%
	S27	3.204	12.190	280.47%
	S26	1.868	4.763	154.91%
	S25	1.856	7.053	280.01%
	S24	1.820	10.911	499.45%
	S23	1.796	12.811	613.13%
	S22	2.436	12.900	429.58%
	S21	1.673	13.244	691.85%
	S20	1.693	13.254	682.69%
	Assessment location	Cumulative Usage Factor		
		Option 1	Option 2	Diff (%)
Outer Surface	S29	0.747	0.747	0.00%
	S28	1.080	1.080	0.00%
	S27	1.270	1.270	0.00%
	S26	0.105	0.113	7.48%
	S25	0.137	0.146	6.69%
	S24	0.265	0.276	4.24%
	S23	0.365	0.365	0.00%
	S22	0.216	0.248	14.82%
	S21	0.814	0.814	0.00%
	S20	0.771	0.771	0.00%

4.3.3 Material Properties

The calculation of S_{alt} also requires consideration of material properties and their variation with temperature. Whilst this was not considered in Benchmark 2 (1), which adopted temperature-independent properties, these factors can potentially influence the results of fatigue calculations.

4.3.3.1 Design stress intensity, S_m

The design stress intensity, S_m, is required for the calculation of the plasticity correction factor, K_e. S_m varies depending on the type of material and the prevailing temperature. The temperature-

dependent S_m values for each material are tabulated within ASME Section II, Part D (13) (or in the case of RCC-M, within Annex ZI 1.0). ASME III Appendix XIII-3420 states:

> *When the secondary stress is due to a temperature transient or to restraint of free end displacement, the value of S_m shall be taken as the average of the tabulated S_m values for the highest and lowest temperatures of the metal (at the point at which the stresses are being analysed) during the transient. When part or all the secondary stress is due to a mechanical load, the value of S_m shall be based on the highest metal temperature during the transient.*

RCC-M also provides equivalent requirements in B 3234.2. Thus, this allows for the use of the average S_m values corresponding to the maximum and minimum temperatures of the transient to be used where no mechanical loads contribute to the secondary stress intensity range. Since stress cycles can arise due to an outside peak-valley pair, the word *'transient'* in this context is somewhat questionable. The interpretation here is that the average S_m value should be obtained by averaging the S_m values determined from the metal temperatures at the peak and valley of the transient pair, or, in the case of mechanically induced secondary stresses, from the maximum of the two metal temperatures. This is the recommended approach here as it more meaningful and straightforward to implement algorithmically since most cycle counting algorithms should be capable of recording the metal temperatures at the peak and valley time points.

4.3.3.2 Representative elastic modulus, E_a

The elastic modulus correction factor, E_{mod} defined in Equation 16, must be calculated to 'correct' the S_{alt} value in accordance with ASME III Appendix XIII-3520 (d). This allows for transferability between the pseudo-stress values determined from the elastic fatigue analysis and the actual value of alternating strain used to derive the design fatigue curves. Appendix XIII-3520 (d) states:

> *Multiply S_{alt} (as determined in XIII-2410 or XIII-2420) by the ratio of the modulus of elasticity given on the design fatigue curve to the value of the modulus of elasticity used in the analysis.*

What constitutes the 'modulus of elasticity used in the analysis' is not explicitly stated in the BPVC. Considering that BPVC also adopts a temperature-dependent approach for S_m, two options are to use the value of E either at the maximum temperature of cycle or at the average temperature of the cycle. Technically speaking, if the calculation of S_{alt} was instead performed based on elastic pseudo-strain intensities calculated using the instantaneous E value at the peak and valley time points, then this would produce the most physically consistent result. These three options are described below in Equation 20, Equation 21 and Equation 22.

$$S_{alt}\ by\ \text{Equation 17}\ with\ E_{mod} = \frac{E_c}{E(max[{}^m t, {}^n t])}$$

Equation 20

$$S_{alt}\ by\ \text{Equation 17}\ with\ E_{mod} = \frac{E_c}{E(average[{}^m t, {}^n t])}$$

Equation 21

$$S_{alt} = \frac{1}{2} K_e E_c \cdot \left[\frac{{}^m\sigma_I}{{}^m E} - \frac{{}^n\sigma_I}{{}^n E}\right] = \frac{1}{2} K_e E_c \cdot [{}^m\varepsilon_I - {}^n\varepsilon_I]$$

Equation 22

Only option 3 is physically relevant since the value of E_a is effectively built into the pseudo-strain intensities determined at the peak and valley of the cycle. The results from options 2 and 3 would however be expected to give quite similar results in most cases, with option 1 producing the most conservative correction. Most of the conservatism in most analyses will arise from the K_e factor. Therefore, it is recommended here to adopt either options 2 or 3 for the calculation of E_a in the interests of reducing excessive conservativism in the fatigue calculations.

4.3.3.3 Effect of assumed material properties on fatigue results

To consider the effect of the input material properties on the final calculation results, several fatigue analyses were conducted for Benchmark 2 considering three different basic assumptions:

- Temperature-independent material properties for the FE stress analysis and fatigue assessment (as in the Benchmark 2 specification (1)).
- Temperature-dependent material properties for the FE stress analysis and fatigue assessment and assuming S_m and E_a corresponding to the maximum temperature of the cycle.
- Temperature-dependent material properties for the FE stress analysis and fatigue assessment but adopting less pessimistic values of S_m and E_a where permitted.

The temperature-dependent physical properties for Type 316L stainless steel specified in Appendix 4, Tables A4.1 and A4.3 of (1) were utilized for the FE stress analysis. The temperature dependent S_m values for Type 316L were obtained from ASME BPVC Section II, Part D, Table 2A (13). It should be noted that ASME has recently provided guidance on a procedure for ferritic and austenitic steels to establish the allowable alternating stress intensity as a function of temperature in ASME Record 17-924 (14).

The total stress intensity range, S_p, calculated at each assessment location is shown in Figure 14 for both transients (T1 and T2) considered in Benchmark 2. The solid markers denoted the results obtained for the inner surface, whilst the open markers denoted the results obtained for the outer surface. As shown, the stress results obtained by considering temperature-dependent material properties were generally found to be more pessimistic than the assumption of elevated temperature fixed material properties. The reason for this is that the elastically calculated stresses are higher in the case of the temperature-dependent properties due to the higher elastic modulus at lower temperatures. The effect of the increased elastic modulus is more pronounced than that of the lesser thermal expansion coefficient, which leads to higher thermal stresses.

The choice of whether to determine S_m and E_a from the maximum temperature of the cycle or to adopt more realistic values (as permitted by the Code rules), can have an important impact on the results of the fatigue assessment. The CUFs calculated at each assessment location are shown in Figure 15, where the solid markers denoted the results obtained for the inner surface whilst the open markers denote the results obtained for the outer surface. Table 4 summarizes the ASME III CUFs obtained for each method at the inner and outer surface. As shown, option 2 produced CUF results that were between 3% higher and 17% less than those of option 1. Option 3 allowed for a slight reduction in CUFs compared to option 2 (up to around 10%) due to the less pessimistic values of S_m and E_a adopted in the fatigue calculations; this represents a significant reduction in the CUFs of typically 15-30% compared to the use of constant elevated temperature material properties.

Overall, the variation of material properties with temperature is a significant consideration in codified elastic fatigue assessments. The results presented here suggest that adopting fixed elevated temperature properties may give a false impression of conservatism regarding finite element stresses, as the total stress intensity range (S_p) was found to be 5-10% higher when temperature-dependent material properties were used. However, when considering the final CUFs obtained from the fatigue assessment, the use of constant elevated temperature properties generally still produced the most conservative results. Whilst the stress ranges calculated using this approach are lower, the more conservative elevated temperature value of S_m adopted still generally leads to a higher K_e factor. Furthermore, the higher value of E_a leads to a more severe elastic modulus adjustment (E_c/E_a), which provides some additional conservatism. Nonetheless, there are still situations where this is not the case (see entries highlighted in red in Table 4). It is therefore recommended that, where possible, temperature-dependent material properties should be employed in the FE stress analysis as this will provide a more realistic representation of component thermo-elastic behaviour.

If temperature-independent properties are necessary, for example when utilizing an analytical solution such as that proposed in (8), then a few choices are available to analysts.

In some cases, it may be more appropriate that fixed temperature properties be chosen such that they maximize stresses, such as for initial fatigue scoping calculations. This can be achieved by selecting properties at specific temperatures such that the product of the elastic modulus and thermal expansion coefficient (E_α) is maximized, and the thermal diffusivity (κ) is minimized. For example, using the materials data specified in Appendix 4 of (1), it is clear that E_α peaks at 50°C whilst κ achieves a minimum at 20°C (see Figure 16); therefore, the use of elastic properties at 50°C and thermal properties at 20°C would be expected to maximize stresses. However, this is likely to be excessively conservative in most situations. Furthermore, it may be difficult to apply reliably to complex structures involving multiple materials. For example, this approach may not be appropriate for PWR Class 1 piping nozzles containing a thermal sleeve, since minimizing the thermal diffusivity of the sleeve material would overestimate its capacity to soak thermal stresses, thereby potentially under-predicting the extent of thermal fatigue damage arising in the nozzle material.

Therefore, if this approach is to be used for complex structures, it is recommended that analysts should undertake a sensitivity study to understand the competing effects of different material properties on fatigue damage.

To reduce excess conservativism, another simple option is to utilize material properties at the mean value of temperature achieved considering all transient events included in the design specification for the component. Adopting such an approach is likely to yield reasonable accuracy in most situations, although the influence of more severe infrequent transients (*e.g.*, Service Level B) is likely to have a disproportionate effect on the calculated mean temperature. If this is undesirable, analysts may instead wish to adopt mean temperature properties that are most representative of the typical range of operating temperatures that are likely to be experienced by the component throughout its service life. This can be achieved by calculating the weighted-average maximum and minimum service temperatures, by weighting the maximum and minimum temperatures attained in each transient according to their contribution to the total design life of the component. As a crude example, consider the following three hypothetical step-change transients characterized by the introduction of cold reactor coolant onto the surface of a component soaking at higher temperature:

Transient 1: 300°C (T_1^{max}) → 21°C (T_1^{min}), 10 design cycles (n_1).

Transient 2: 288°C (T_2^{max}) → 245°C (T_2^{min}), 40,000 design cycles (n_2).

Transient 3: 260°C (T_3^{max}) → 190°C (T_3^{min}), 2,000 design cycles (n_3).

In this crude example, the design life of the component is

$n_t = n_1+n_2+n_3 = 10 + 40{,}000 + 2{,}000 = 42{,}010$ cycles.

The weighted-average maximum and minimum service temperatures, T_w^{max} and T_w^{min}, are

$$T_w^{max} = (n_1/n_t) * T_1^{max} + (n_2/n_t) * T_2^{max} + (n_3/n_t) * T_3^{max}$$
$$= (10/42010) * 300 + (40000/42010) * 288 + (2000/42010) * 260 = 286.67°C$$

$$T_w^{min} = (n_1/n_t) * T_1^{min} + (n_2/n_t) * T_2^{min} + (n_3/n_t) * T_3^{min}$$
$$= (10/42010) * 21 + (40000/42010) * 245 + (2000/42010) * 190 = 242.33°C$$

The weighted-average mean service temperature, T_w^{mean}, is therefore:

$$T_w^{mean} = ½ * (T_w^{max} + T_w^{min}) = ½ * (286.67 + 242.33) = 264.5°C$$

Thus, in this hypothetical example, the analyst could adopt material properties corresponding to 264.5°C and provide rational justification for doing so based on the above weighting methodology.

Finally, in the fatigue assessment, the calculation approach adopted for E_a and S_m (option 2 vs. option 3 stated above) may also influence calculated fatigue usage. The choice of temperature upon which to base E_a is a matter of analyst judgement, as no explicit provisions are included in ASME BPVC Section III, Appendix XIII; on the other hand, the calculation approach adopted for S_m will be driven by satisfying code requirements (*e.g.*, Appendix XIII-3420), and therefore there is relatively little analyst flexibility. Overall, the difference in the results is expected to be relatively modest in practical cases.

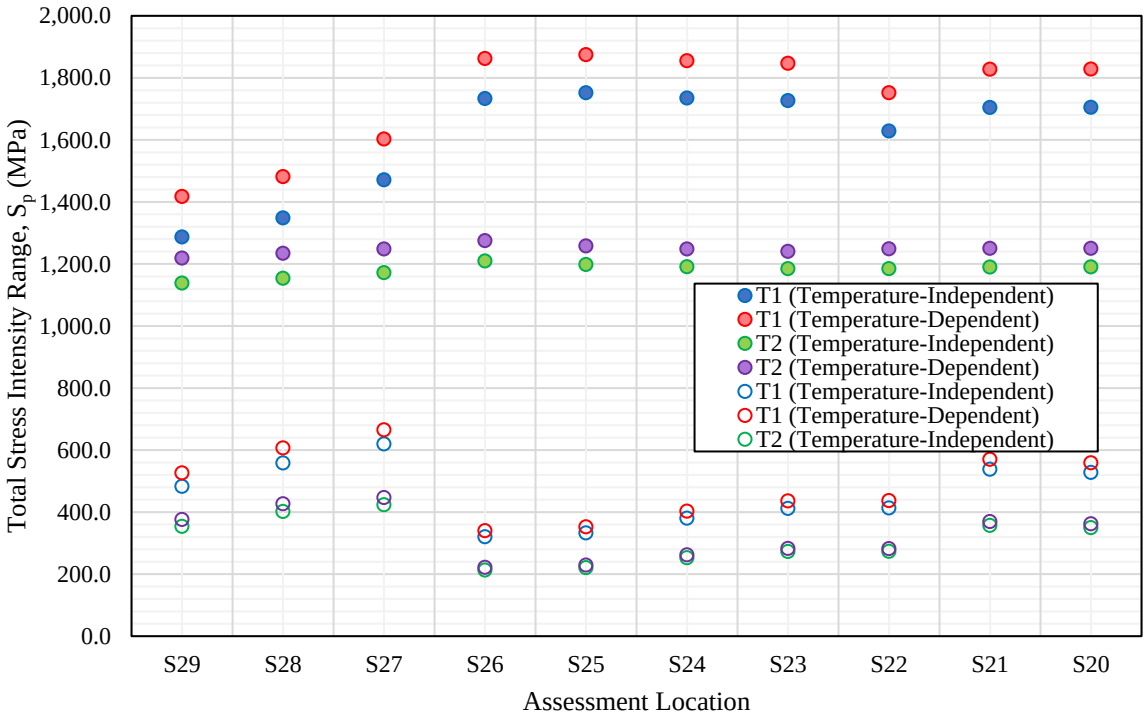

Figure 14. Variation of total stress intensity range S_p, depending on material properties adopted in FE stress analysis

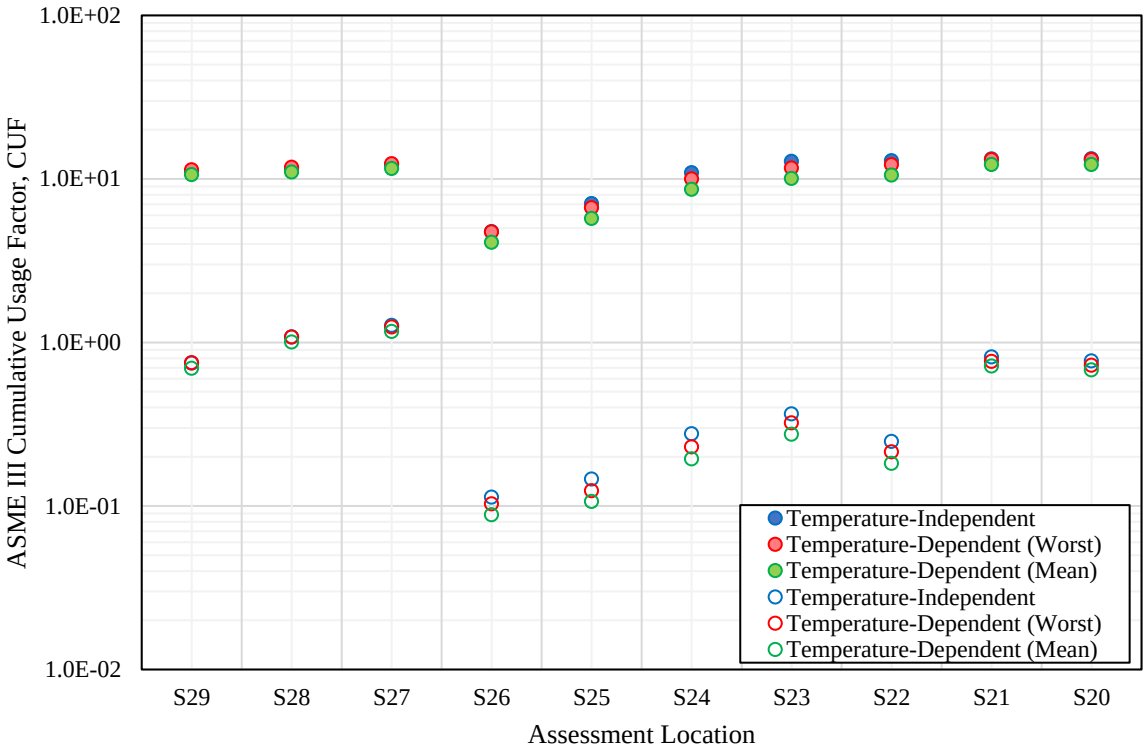

Figure 15. Variation of ASME III CUFs depending on material properties and treatment of temperature

Table 4. Summary of ASME III CUFs depending on adopted material properties and temperature-dependence

	Assessment location	Cumulative Usage Factor				
		Temperature independent (TI)	Temperature dependent (TD) (Avg.)	Temperature dependent (TD) (Worst)	% Diff. [TD Avg. vs. TI]	% Diff. [TD Worst. vs. TI]
Inner surface	S29	11.083	10.613	11.352	-4.24%	2.43%
	S28	11.517	11.015	11.786	-4.36%	2.34%
	S27	12.190	11.558	12.369	-5.19%	1.46%
	S26	4.763	4.087	4.736	-14.19%	-0.57%
	S25	7.053	5.727	6.662	-18.80%	-5.55%
	S24	10.911	8.618	9.995	-21.01%	-8.39%
	S23	12.811	10.048	11.636	-21.57%	-9.18%
	S22	12.900	10.552	12.206	-18.20%	-5.38%
	S21	13.244	12.237	13.113	-7.60%	-0.99%
	S20	13.254	12.244	13.121	-7.62%	-1.01%
	Assessment location	Cumulative Usage Factor				
		Temperature independent (TI)	Temperature dependent (TD) (Avg.)	Temperature dependent (TD) (Worst)	% Diff. [TD Avg. vs. TI]	% Diff. [TD Worst. vs. TI]
Outer surface	S29	0.747	0.695	0.751	-6.98%	0.52%
	S28	1.080	1.004	1.078	-7.03%	-0.14%
	S27	1.270	1.166	1.241	-8.18%	-2.33%
	S26	0.113	0.088	0.103	-21.97%	-9.05%
	S25	0.146	0.106	0.124	-27.02%	-15.17%
	S24	0.276	0.194	0.230	-29.76%	-16.79%
	S23	0.365	0.274	0.322	-24.98%	-11.91%
	S22	0.248	0.182	0.214	-26.60%	-13.73%
	S21	0.814	0.716	0.765	-12.11%	-6.03%
	S20	0.771	0.678	0.725	-12.03%	-5.93%

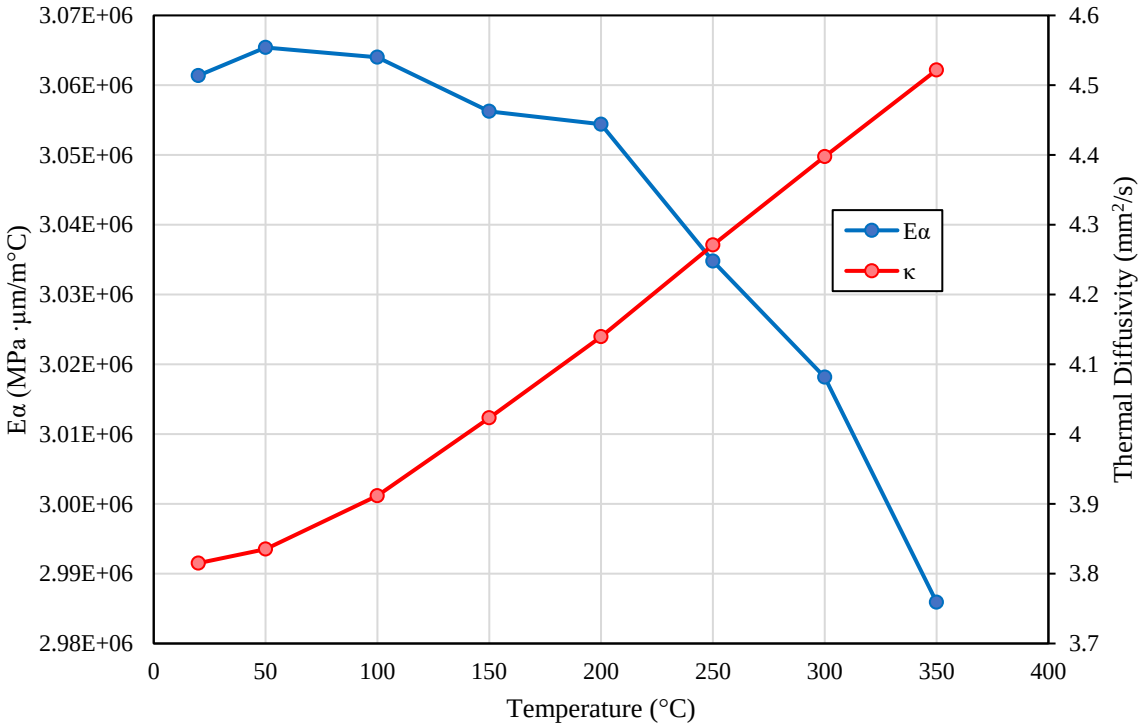

Figure 16. Variation of E_α and κ vs. temperature (°C) based on materials data for Type 316L specified in Appendix 4 of (1)

4.3.3.4 Consideration of mean stress correction at elevated temperature

The superposition of a steady mean stress on a fluctuating stress can produce a significant reduction in high-cycle fatigue endurance. Mean stresses may arise in pressure vessel components from several sources, including sustained mechanical loads (*e.g.*, pressure) as well as residual stresses induced by welding or surface treatment, which may either be beneficial (compressive) or detrimental (tensile) to fatigue life. Such stresses are apt to change over time; displacement-controlled stresses may also relax altogether should a component experience significant plastic cycling. Nonetheless, the actual magnitude of mean stress present within a component at a given moment is fraught with uncertainty.

Rather than try to predict the mean stress, it is more practical and safer to perform fatigue calculations using a derived endurance curve based on fully reversed strain cycling but adjusted downwards at the high-cycle end to allow for the maximum possible effect of mean stress. This is the approach adopted by most recognized nuclear design and construction codes (including ASME III and RCC-M).

With ASME III in particular, the Mandatory Appendix I design fatigue curves contain inherent margin from the use of transference design factors to translate the 'best-fit' strain-life endurance data to a curve that allows for maximum mean stress, size effects, surface finish, data scatter, *etc*., for application to plant components. A modified Goodman correction was applied to the best-fit data to account for the maximum effect of mean stress prior to accounting for the various other design factors, including the factor of 2.0 on alternating stress which dominates in the high-cycle regime.

The modified Goodman approach used in ASME III is shown by Equation 23, where S_N is the permissible fully reversed alternating stress, S_y^c and S_u^c represent the cyclic yield and ultimate tensile strengths of the applicable material, respectively, and S'_N denotes the adjusted alternating

stress after correcting for mean stress. Implicit in Equation 23 is the assumption of a yield-level mean stress, and thus S'_N represents the required magnitude of fully reversed alternating stress that would result in the equivalent fatigue damage as S_N acting in combination with a superimposed mean stress of S_y^c.

$$S'_N = S_N \frac{\left(S_u^c - S_y^c\right)}{\left(S_u^c - S_N\right)} \; if \; S_N \; \leq S_y^c$$
$$S'_N = S_N \;\; if \; S_N > S_y^c$$

Equation 23

The severity of the Goodman correction depends heavily on the assumed cyclic yield strength, S_y^c, and to a lesser extent on the cyclic ultimate strength, S_u^c. The high-cycle regime of the ASME III Appendix I design fatigue curves is based on Equation 23, assuming room temperature values of S_y^c and S_u^c. This is a conservative assumption since adopting a higher room temperature value of S_y^c implies an unrealistically large range of elastic behaviour when extended to high temperatures, wherein mean stresses may be retained under strain cycling; in actuality, the typical values of S_y^c and S_u^c will be lower for the range of temperatures experienced under plant transient fatigue loading. It is noteworthy that ASME III Appendix XIII-3520(d) mandates that the permissible stress amplitude, S_a, be corrected to account for temperature by multiplying by the ratio of the reference Young's modulus of the fatigue curve, E_c, to the Young's modulus at temperature, E_a. The fact that temperature-dependence of the Young's modulus is accounted for therefore also suggests that the mean stress correction should be based on temperature-dependent values of S_y^c and S_u^c, as this appears to be more closely aligned with the ethos of the Appendix XIII-3520 fatigue assessment philosophy.

Furthermore, it has been suggested (15) that the design factor of 2.0 on stress is composed partially of a sub-factor of 1.15 associated with 'environment', which is interpreted to mean the exposure to higher temperatures than would be experienced under room temperature laboratory-controlled conditions. This would therefore also suggest that there is an element of 'double counting' for the effect of temperature when the elastic modulus correction (discussed in Section 0) is applied on top of the existing temperature sub-factor of 1.15 that is already 'built in' to the design fatigue curve. Hence, the adoption of a more realistic temperature-dependent mean stress correction approach at elevated temperatures would also help to offset some of the excess conservatism associated with the elastic modulus correction.

To this end, an ASME Code Case has recently been proposed (C&S Connect Record 17-924) by the Section III Working Group on Fatigue Strength (WGFS), which establishes adjusted design fatigue curves using a modified Goodman correction based on temperature-dependent values of S_y^c and S_u^c, but whilst maintaining the design factors on stress and life (14). The technical basis for the methodology outlined in (14) is extensively detailed within a programme of work published by the Electric Power Research Institute (EPRI) in (17). The methodology proposed in Record 17-924 is briefly summarized here with aid of an example calculation. A more comprehensive exploration of methods to account for mean stress effects in fatigue assessments of pressure vessel components is to be included in a future CORDEL MCSTF report (Fatigue Life Analysis Part 2).

In Section 3 of Record 17-924, the temperature-dependence of S_y^c and S_u^c is assumed to follow the same trend with temperature as their monotonic strength counterparts, S_y and S_u, tabulated in ASME II, Part D, Tables Y-1 and U (13), respectively. This is shown by Equation 24, where the subscript T_r denotes the strength value at room temperature and T denotes the strength value at

temperature. This allows $S^c_{y,T}$ and $S^c_{u,T}$ to be determined across the full range of temperatures for which $S_{y,T}$ and $S_{u,T}$ are known from (13).

Figure 17 shows an example of the trend in $S^c_{y,T}$ and $S^c_{u,T}$ versus temperature for austenitic stainless steel (SA-312 TP304) established using Record 17-924. The specified cyclic yield and ultimate tensile strength at room temperature, S^c_{y,T_r} and S^c_{u,T_r}, for austenitic stainless steel are provided in Table 1 of ASME Record 17-924 (14) as 303 MPa and 648 MPa, respectively. These values are used in the austenitic stainless steel design fatigue curve (ASME III Appendix I-9.2) and are derived from the work of Jaske & O'Donnell (18).

$$S^c_{y,T} = S^c_{y,T_r}\frac{S_{y,T}}{S_{y,T_r}}$$
$$S^c_{u,T} = S^c_{u,T_r}\frac{S_{u,T}}{S_{u,T_r}}$$

Equation 24

In Section 4 of Record 17-924, the procedure to determine the adjusted permissible alternating stress amplitude (S_R) based on the temperature-dependent Goodman correction is described. First, the mean fatigue curve is inferred from the design fatigue curve (which includes the factor of 2.0 on stress in the high-cycle regime), by removing the effect of the room temperature Goodman correction. The permissible fully reversed alternating stress, S_N, for a given temperature, T, and associated number of cycles, N, is calculated by Equation 25. If S_N exceeds S^c_y, the effect of mean stress will be negligible due to relaxation upon plastic cycling, and thus the existing value of alternating stress associated with the design fatigue curve, S_a, remains applicable in this situation.

$$S_{N,T_r} = \frac{2S^c_{u,T_r}S_a}{S^c_{u,T_r} - S^c_{y,T_r} + 2S_a} \; for\; S_{N,T_r} \le S^c_{y,T_r}$$
$$S_{N,T} = \frac{2S^c_{u,T}S_a}{S^c_{u,T} - S^c_{y,T} + 2S_a} \; for\; S_{N,T} \le S^c_{y,T}$$

Equation 25

The mean stress correction for room temperature T_r and at temperature T are calculated according to Equation 26.

$$MSC_{T_r} = \frac{S^c_{u,T_r} - S^c_{y,T_r}}{S^c_{u,T_r} - S_N} \; where\; MSC_{T_r} \le 1.0$$
$$MSC_T = \frac{S^c_{u,T} - S^c_{y,T}}{S^c_{u,T} - S_N} \; where\; MSC_T \le 1.0$$

Equation 26

The new value of alternating stress, S_R, based on the temperature-dependent Goodman correction is then calculated by Equation 27.

$$S_R = S_a \cdot \left(\frac{MSC_T}{MSC_{T_r}}\right)$$

Equation 27

After S_R is determined, this must then be multiplied by the ASME III Appendix XIII-3520 (d) elastic modulus correction factor, E_c/E_a, prior to evaluating the fatigue usage. To ensure consistency in

the adopted temperature-dependent properties, Record 17-924 requires that the temperature used for determining S_R should be the same as that used to calculate the representative elastic modulus of the fatigue cycle, E_a. Therefore, there is a good degree of flexibility to the procedure, given that Appendix XIII-3520 does not explicitly state what value to adopt for E_a; thus, Record 17-924 could be applied using either of the characteristic cycle temperatures (mean or maximum metal temperature) described in Section 0 for calculating E_a (see Equation 20 and Equation 21).

Figure 18 shows as a representative example the adjusted design fatigue curves generated using the approach described in Record 17-924 for SA-312 TP 304 stainless steel at several characteristic temperatures. At room temperature (~20°C), the adjusted curve is equivalent to the Appendix I-9.2 design fatigue curve. At higher temperatures, there is a clearly observable benefit from using the temperature-dependent Goodman correction; an increase in the permissible stress amplitude by around 10-20% is achievable beyond 10^6 cycles for the range of operating temperatures typical of LWR plants (288-325°C). The fatigue limit at 320°C (114 MPa) calculated using the temperature-dependent mean stress correction is approximately 22% higher than that of the existing Appendix I-9.2 design fatigue curve (93.7 MPa).

Practical examples of where Record 17-924 would be expected to improve the fatigue evaluation of pressure vessel components include:

- The assessment of high frequency loading such as those arising from flow induced vibration and thermal stratification, which may be associated with a very large number of cycles that cannot be reasonably predicted. An infinite life approach is usually appropriate for these events, by comparing the predicted stress amplitude with the fatigue limit at 10^{11} cycles. The increase in the fatigue limit at elevated temperatures permitted by Record 17-924 will therefore offer some additional margin on the threshold stress amplitude beyond which the effect of these high frequency loading events must be considered.

- The assessment of other fatigue cycles associated with the high-cycle finite life regime (10^6-10^{11} cycles). In particular, cycles possessing a low stress amplitude, but with a slow tensile strain rate and high metal temperature (and therefore high peak stress) will benefit most in terms of a reduction in excess fatigue usage from the application of Record 17-924.

The methodology proposed in Record 17-924 represents a considerable improvement to the treatment of mean stresses in traditional ASME III fatigue assessments, in terms of both practicality and accuracy. As the methodology retains the modified Goodman framework, it is largely a refinement of the existing approach rather than a fundamental change to fatigue design philosophy. It is therefore expected that Record 17-924 will receive approval from the ASME Board on Nuclear Codes and Standards (BNCS) for publication as an ASME Section III Code Case in the near future. It is recommended that this future Code Case be applied where appropriate in ASME III fatigue assessments to permit a more accurate evaluation of mean stresses at elevated temperature.

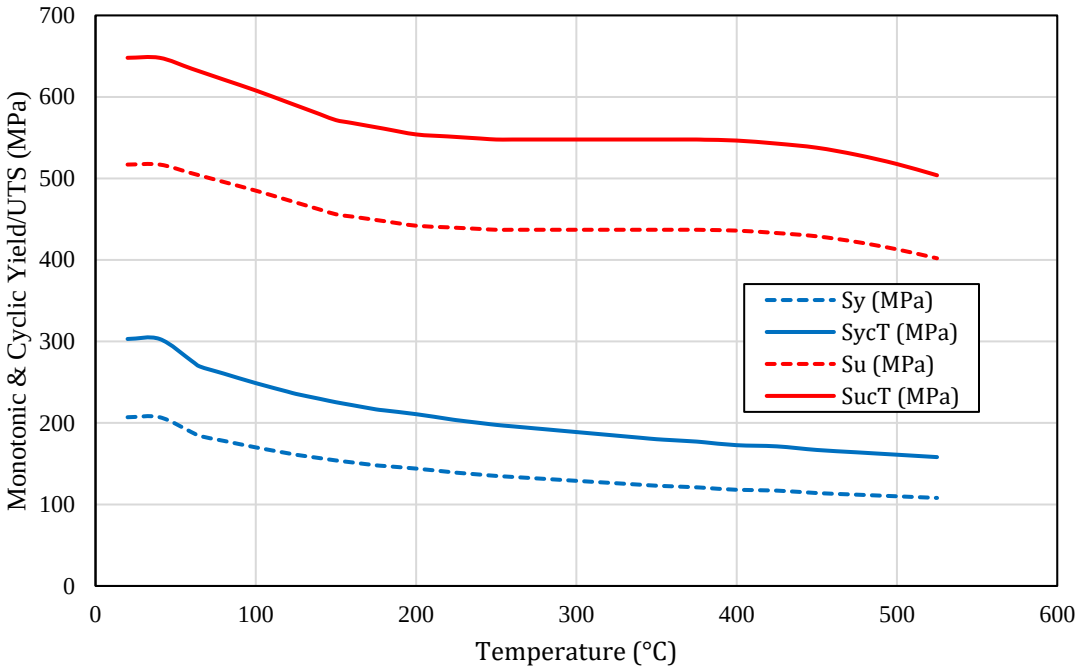

Figure 17. Example of temperature-dependence of S_y^c and S_u^c established for SA-312 TP304 material from Record 17-924. Dashed lines show monotonic strength; solid lines show corresponding cyclic strength

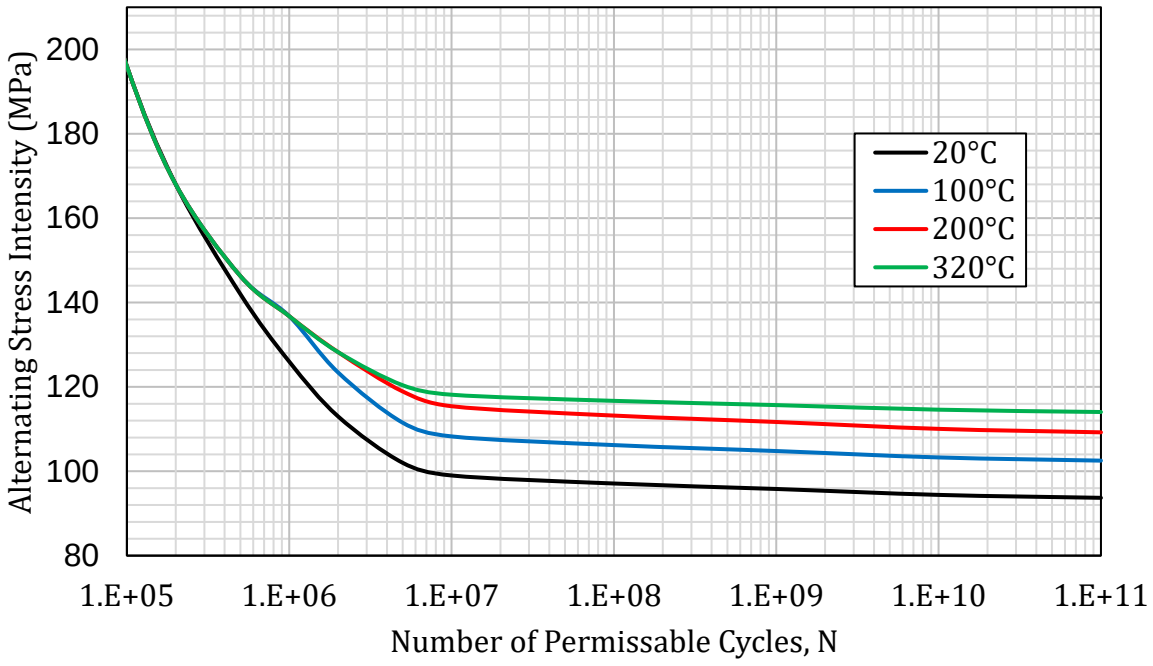

Figure 18. Example of adjusted design fatigue curves for SA-312 TP304 based on the temperature-dependent Goodman correction approach proposed in Record 17-924

4.3.4 Considerations specific to RCC-M B-3200

Several considerations that were highlighted from the RCC-M approach are briefly discussed here, specifically for austenitic stainless steels and inconels.

4.3.4.1 Generalized calculation of the plasticity correction factor K_e

In RCC-M B-3234.6, two plasticity correction factors are prescribed for austenitic stainless steels and inconels. S_{alt} is calculated as one-half times the sum of the plasticity-corrected mechanical and thermal contributions to the total stress range:

$$S_{alt} = \frac{1}{2} \cdot \left[K_e^{mech} S_p^{mech} + K_e^{ther} S_p^{ther} \right]$$

Equation 28

Where K_e^{mech} is the correction applied to the mechanical portion of the total stress range, S_p^{mech}, and is equivalent to the ASME III Appendix XIII-3450 K_e described by Equation 15. K_e^{ther} is the correction applied to the thermal portion of the total stress range S_p^{ther}, and is determined according to Equation 29 for austenitic stainless steels and inconels:

$$K_e^{ther} = max\left(1.0, \quad 1.86 \left[1 - \frac{1}{1.66 + \frac{S_n}{S_m}} \right] \right)$$

Equation 29

Importantly, the RCC-M K_e^{ther} factor is greater than unity for $S_n/S_m \geq 0.51$ and therefore applies even where S_n remains within the elastic range. Thus, the RCC-M K_e factor is greater than the ASME III K_e factor for $S_n \leq 3S_m$ and tends asymptotically to a value of 1.86 for $S_n >> 3S_m$. Figure 19 shows the RCC-M K_e^{mech} and K_e^{ther} correction curves for austenitic stainless steels and inconels.

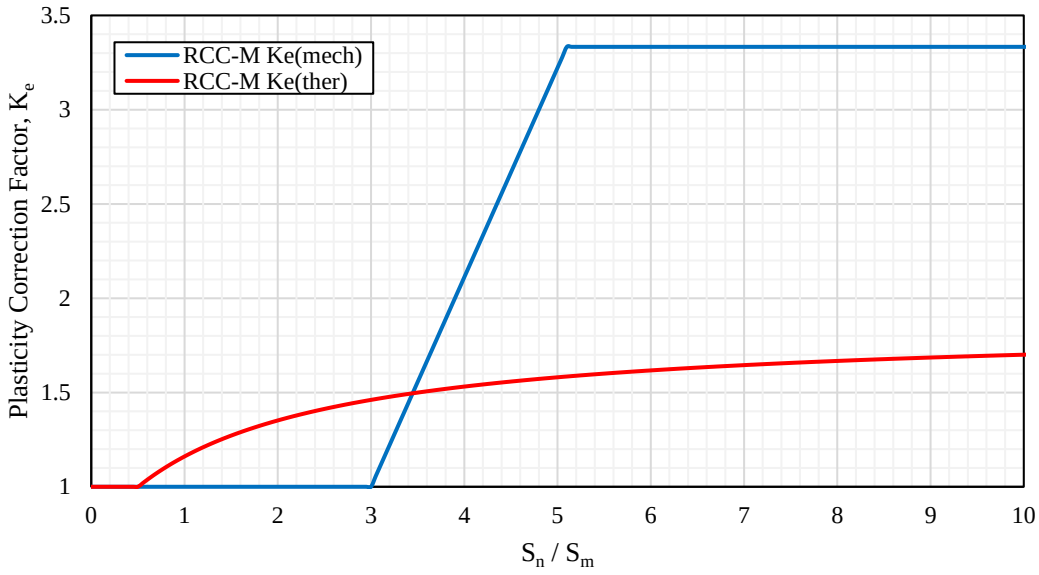

Figure 19. K_e^{mech} and K_e^{ther} prescribed in RCC-M B 3234.6 for austenitic stainless steels and inconels.

To enable a direct comparison between code K_e methods that involve more than a single correction factor, and which depend on multiple different stress ranges, an equivalent correction factor, $K_{e,eq}$, must be determined. The purpose of $K_{e,eq}$ is to reduce the combined effect of multiple plasticity correction factors to a single value whose effect on S_{alt} is equivalent, and it serves as the basis for comparison of all plasticity correction methods. $K_{e,eq}$ is calculated according to Equation 30.

$$K_{e,eq} = \frac{2 \cdot S_{alt}}{S_p} \cdot \frac{E_a}{E_c}$$

Equation 30

In the case of purely thermal loading, $K_{e,eq}$ will be equal to K_e^{ther}. For combined thermal-mechanical loading, $K_{e,eq}$ represents the weighted-average of K_e^{mech} and K_e^{ther}. This calculation enables a simple comparison to be made between the ASME and RCC-M plasticity correction methods, and indeed the K_e factors derived from elastic-plastic FEA.

4.3.4.2 Calculation of S_p^{mech} and S_p^{ther} under combined loading

A further consideration is the method used to determine S_{alt} under combined loading. In general, there are three possible methods for the calculation of S_{alt}, which are highlighted by Equation 31, Equation 32 and Equation 33.

$$S_{alt} = 0.5 \cdot \frac{E_c}{E} \cdot \max_{ij} \left(\{K_e^{mech}\}_{ij} \{S_p^{mech}\}_{ij} + \{K_e^{ther}\}_{ij} \{S_p^{ther}\}_{ij} \right)$$

Equation 31

$$S_{alt} = 0.5 \cdot \frac{E_c}{E} \cdot \max_{ij} \left(K_e^{mech} \{S_p^{mech}\}_{ij} + K_e^{ther} \{S_p^{ther}\}_{ij} \right)$$

Equation 32

$$S_{alt} = 0.5 \cdot \frac{E_c}{E} \cdot \left(K_e^{mech} \max_{ij} \{S_p^{mech}\}_{ij} + K_e^{ther} \max_{i'j'} \{S_p^{ther}\}_{i'j'} \right)$$

Equation 33

Neither S_p^{mech} nor S_p^{ther} are defined in ASME III, and therefore these calculation options are only relevant to RCC-M codified fatigue assessments. Only Equation 32 and Equation 33 are explicitly defined in RCC-M, but all three represent feasible approaches. In each of these options, K_e^{mech} and K_e^{ther} are always calculated based on the maximum S_n for the cycle.

The use of Equation 31 is less conservative but also more time-consuming since it requires the scanning of the stress-time history to determine different time combinations to obtain the combination that maximizes S_{alt}. Whilst this a viable approach, and similar approaches have been proposed in other technical publications (19), it is not considered further here.

The difference between Equation 32 and Equation 33 concerns the time points used for determination of S_p^{mech} and S_p^{ther}. Equation 32 considers the maximum S_{alt} formed from S_p^{mech} and S_p^{ther} based on only a single pair of time points corresponding to maximum S_p. Equation 33 on the other hand considers two pairs of time points for both S_p^{mech} and S_p^{ther}, and therefore aims to determine the maximum S_{alt} based on independent maximization of S_p^{mech} and S_p^{ther}.

RCC-M defines the calculation of S_p^{mech}:

> *Range of the mechanical part of the stresses, $(S_p(1))_{ij}$ between the two instants i and j or the maximum value of the mechanical part during the transient.*

And likewise, for the calculation of S_p^{ther}:

> *Range of the thermal part of the stresses $(S_p(1))_{ij}$, between the two instants i and j or the maximum value of this thermal part during the transient […] it is acceptable to take as the value of S_p^{ther}, the difference between the total S_p and S_p^{mech} adopted above.*

Thus, RCC-M effectively gives two options for the calculation of S_p^{ther}:

1. Calculation of S_p^{ther} based on the total stress history considering only thermal loads.
2. Calculation of S_p^{ther} as simply the difference between the total stress range considering both superimposed mechanical and thermal loads less the total stress range arising due to mechanical loads only:

$$S_p^{ther} = \max_{ij}\{S_p\} - \max_{i'j'}\{S_p^{mech}\}$$

Equation 34

It has been found that option 2 can lead to less conservative results than option 1 in situations where the mechanical and thermal stresses vary out-of-phase. This was evidenced for the results obtained for T2 of Benchmark 2 (1), where significant differences arose depending on whether option 1 or 2 was used. To illustrate this, consider the mechanical, thermal, and total stress intensity variations obtained at the inner point of S22 (nozzle crotch corner) for Transient T2 Figure 20, where this effect showed the greatest significance. Since T2 considered a pressure drop out-of-phase with a thermal shock, the use of option 1 independently accounts for both S_p^{ther} and S_p^{mech} despite both stress histories being out-of-phase. On the other hand, option 2 would be expected to predict a lower value of S_p^{ther} and consequently lead to a less conservative prediction of S_{alt}. The S_{alt}, $K_{e,eq}$, and FUF obtained for T2 considering both RCC-M options 1 and 2 are shown respectively in Figure 21, Figure 22 and Figure 23. The solid markers denote the results obtained for the inner surface, whilst the open markers denote the results obtained for the outer surface.

As can be seen from Figure 21, the use of option 1 leads to the calculation of higher S_{alt} values in all cases. Importantly, the locations where S_{alt} is at a maximum are different for both options. Option 1 predicts the maximum S_{alt} to be at the nozzle crotch corner (S22). Option 2 on the other hand predicts the maximum S_{alt} (and therefore highest fatigue damage) at the nozzle-to-pipe juncture (S27) and the MCL (S20, S21). The difference in S_{alt} calculated using both options was found to be greatest at the inner point of S22, where S_{alt} calculated by option 1 was 23% higher than option 2.

As shown by Figure 22, a similar trend to S_{alt} was observed for the equivalent plasticity correction factor, $K_{e,eq}$, calculated by Equation 30, though $K_{e,eq}$ is generally higher on the outer surface (except for S22). The difference in $K_{e,eq}$ observed from both calculation options was found to be greatest for the branch pipe (S27-S29), nozzle crotch corner (S22), and MCL (S20, S21) regions. The differences were not as pronounced in the nozzle region (S23-S27).

As shown in Figure 23, the choice of calculation option for S_p^{mech} and S_p^{ther} can have a quite dramatic effect on the calculated FUF. Due to the non-linearity of the design fatigue curve in the low-cycle regime, the effect on the FUF is more pronounced than for S_{alt}. Table 5 summarizes the FUFs calculated for Transient 2 considering both RCC-M calculation options. On the inner surface, difference in FUFs is greatest for S22, which is 85% higher in the case of option 1 compared to option 2. On the outer surface, the difference in FUFs is generally higher, and found to be greatest for S21, which is 221% higher for option 1 compared to option 2.

The analysis presented herein highlights the crucial importance of the methodology adopted for the calculation of S_p^{mech} and S_p^{ther}, and its potential to significantly affect the calculated FUF in RCC-M fatigue calculations. It should however be noted that Benchmark 2 represents a rather extreme example, and the differences in the results observed for both calculation options are likely to be less pronounced in practice.

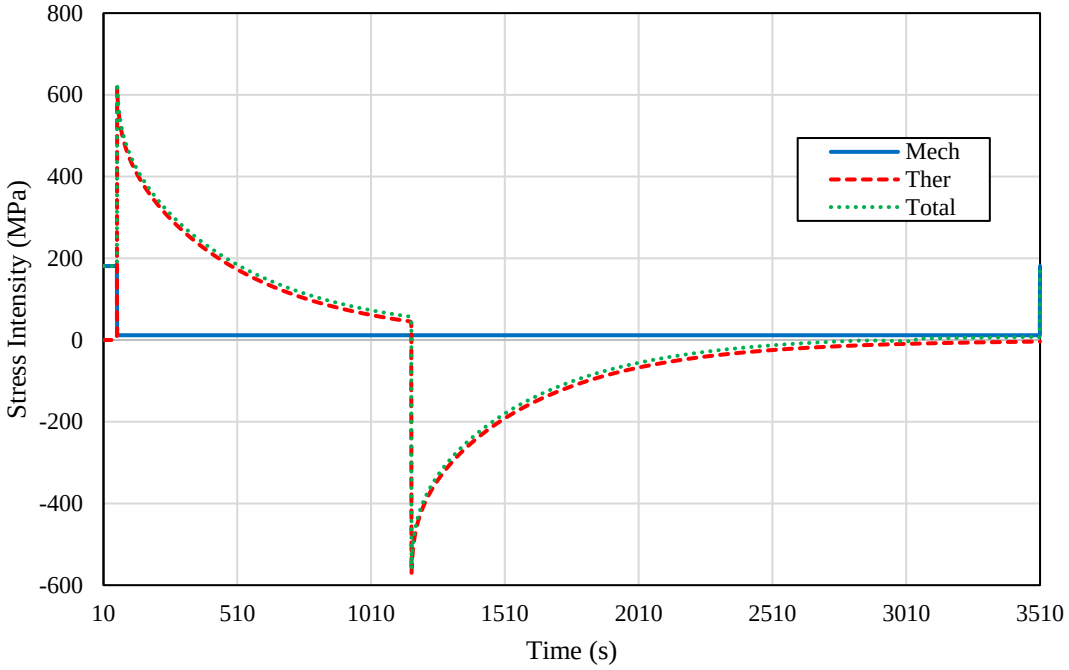

Figure 20. Variation of mechanical, thermal, and total stress intensity at SCL 8 (inner) for T2

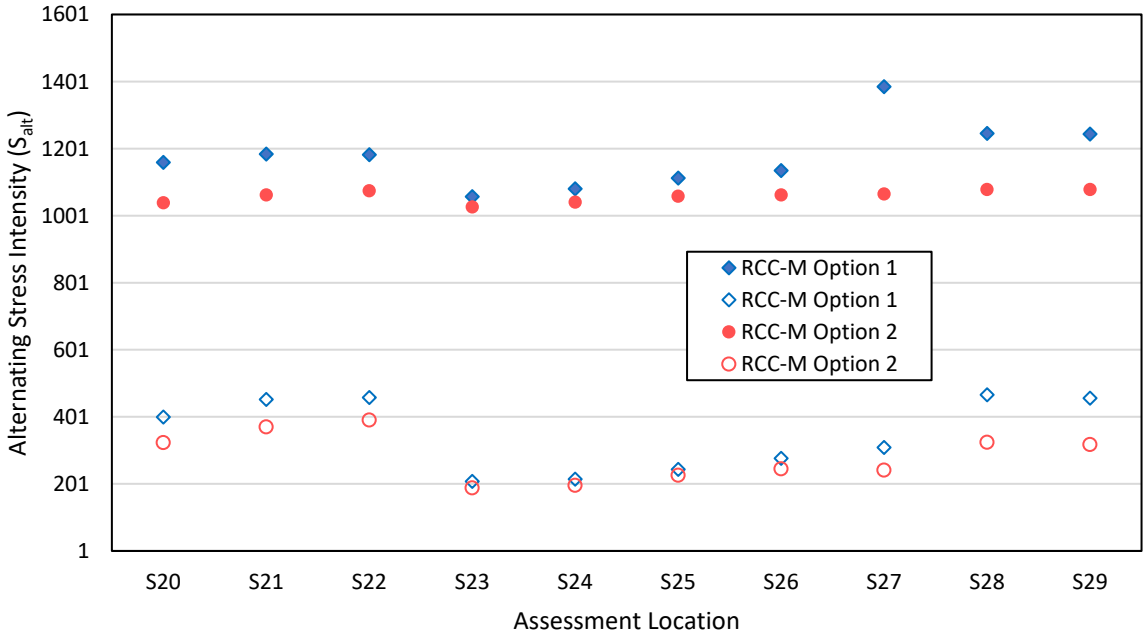

Figure 21. Variation in calculated S_{alt} for Transient 2 based on RCC-M calculation option for S_p^{mech} and S_p^{ther}

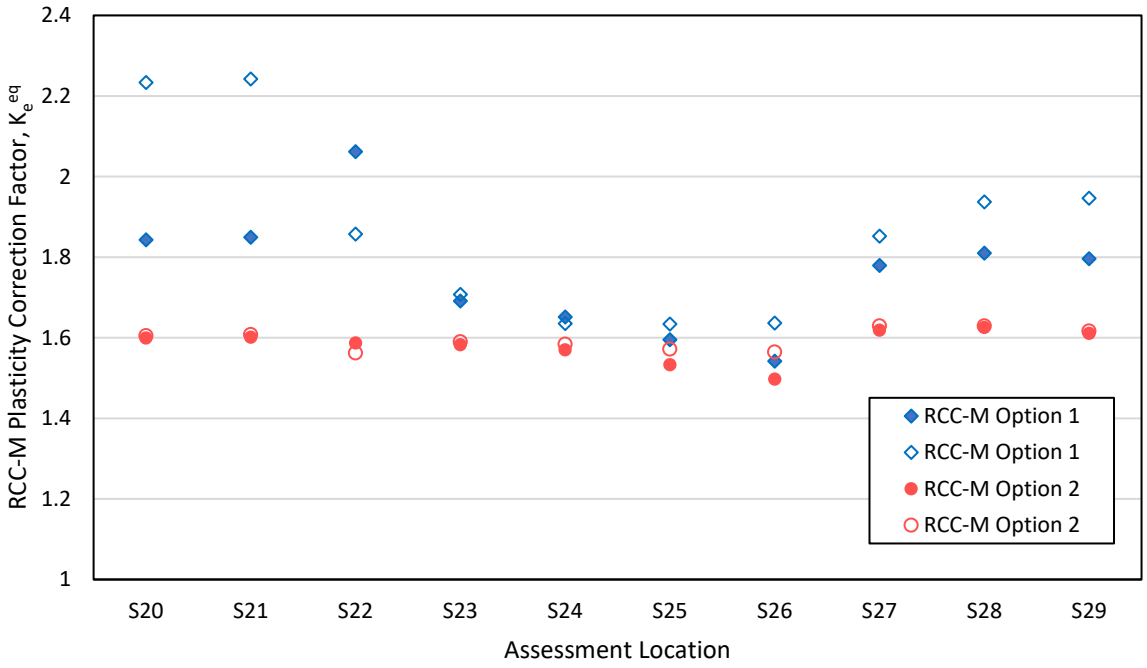

Figure 22. Variation in calculated $K_{e,eq}$ for Transient 2 based on RCC-M calculation option for S_p^{mech} and S_p^{ther}

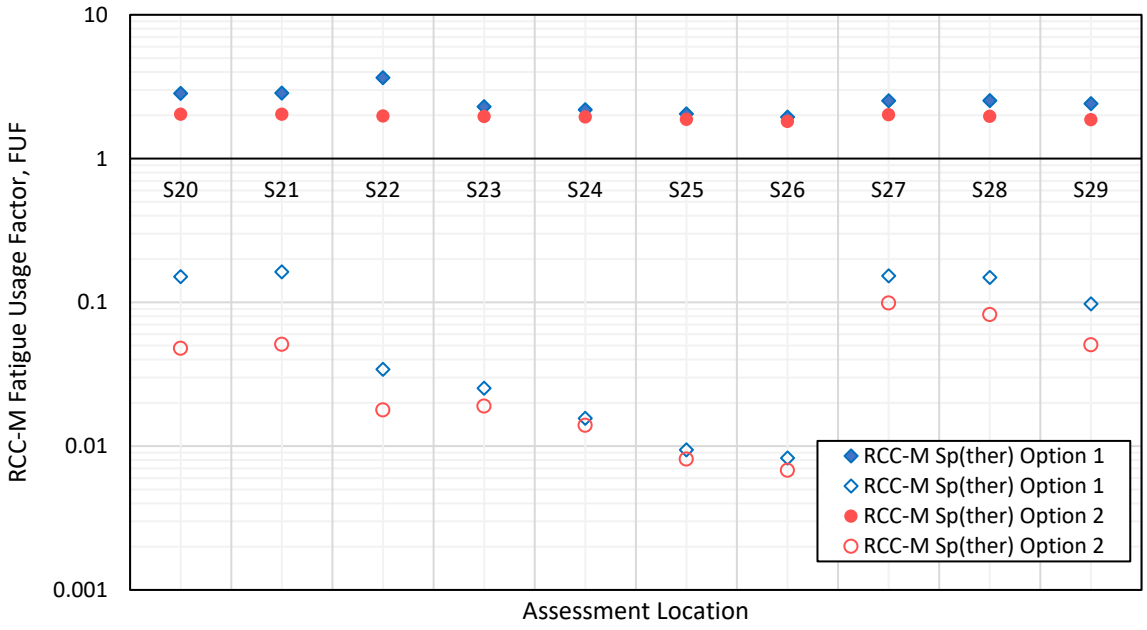

Figure 23. Variation in calculated FUF for Transient 2 based on RCC-M calculation option for S_p^{mech} and S_p^{ther}

Table 5. Summary of FUFs for Transient 2 based on RCC-M calculation option for S_p^{mech} and S_p^{ther}

	Assessment Location	Fatigue Usage Factor		
		Option 1	Option 2	Diff (%)
Inner Surface	S29	2.410	1.863	-29.37%
	S28	2.531	1.964	-28.92%
	S27	2.523	2.018	-25.03%
	S26	1.943	1.811	-7.26%
	S25	2.044	1.871	-9.27%
	S24	2.189	1.948	-12.39%
	S23	2.293	1.962	-16.87%
	S22	3.655	1.976	-84.99%
	S21	2.851	2.034	-40.19%
	S20	2.841	2.034	-39.64%
	Assessment Location	Fatigue Usage Factor		
		Option 1	Option 2	Diff (%)
Outer Surface	S29	0.098	0.051	-92.84%
	S28	0.149	0.082	-81.37%
	S27	0.153	0.099	-54.68%
	S26	0.008	0.007	-21.65%
	S25	0.009	0.008	-16.08%
	S24	0.016	0.014	-12.05%
	S23	0.025	0.019	-33.44%
	S22	0.034	0.018	-91.55%
	S21	0.163	0.051	-219.45%
	S20	0.151	0.048	-215.04%

4.4 Summary

This section has drawn attention to several factors relevant to codified elastic fatigue analysis pursuant to ASME BPVC Section III Appendix XIII-3520 (20) and RCC-M Volume B-3200 (4). The common factors to both codes addressed in this report included the stress linearization technique, selection of relevant stress states (time-pairs) for calculation of S_n, and the definition of temperature-dependent material properties. These factors are not explicitly addressed within the code rules and are often a matter of analyst judgement. Additionally, factors specific to RCC-M including the correct way to compute the equivalent plasticity correction factor, $K_{e,eq}$, and the methodology adopted for determining S_p^{mech} and S_p^{ther} were also considered. Recommendations for addressing the above factors in fatigue calculations have also been provided where appropriate.

5. Plastic fatigue analysis recommendations

This final section provides recommendations for the analysis of plastic fatigue. It considers existing approaches for examining the effects of the cyclical thermal and mechanical loads that Class 1 nuclear components are subjected to over the course of their lifetime and how the choice of material properties influences the outcome of analyses.

Fatigue analysis requires the total strain range, $\Delta\varepsilon_t$, to be evaluated for each combination of operating conditions. The codified fatigue curves are based on strain-controlled low cycle fatigue testing but, for practical reasons and ease of use, fatigue curves are translated into a 'fictive' stress range S_{alt} (*i.e.*, pseudo elastic stress range) via the reference modulus of elasticity E_c, which is associated with the fatigue curve.

$$S_{alt} = \frac{1}{2} E_c \, \Delta\varepsilon_t$$

Equation 35

In the linear fatigue approach, this total strain range is deduced from the elastic strain range ($\Delta\varepsilon_e = Sp/E$), assessed under the same conditions. Strain and stress are no longer proportional beyond the yield strength, and it is therefore necessary to consider the effect of plasticity via an fatigue plasticity correction factor K_e.

$$S'_{alt} = \frac{1}{2} E_c \, K_e \frac{S_p}{E}$$

Equation 36

Non-linear fatigue analysis can therefore be performed following two different approaches:

- Approach A: direct elastic-plastic analysis (see Section 5.3)

  For a given condition, a direct analysis is performed, determining directly through calculation the ranges of elastic-plastic strain.

- Approach B: elastic-plastic amplification assessment (see Section 0)

  For a given condition, a new K_e factor can be assessed to refine the plastic corrections in the linear fatigue analysis.

5.1 Strain calculation and analysis

The total elastic-plastic strain range $\boldsymbol{\Delta\varepsilon_t}$ can be directly assessed from a non-linear cyclic calculation with an adapted behaviour law (non-linear strain hardening model, see Section 5.2). A single cycle is sufficient when the behaviour law has been identified via the reduced cyclic curve. In the other cases, the calculation must be performed until cycle stabilization.

An analysis based on monotonic calculation with an isotropic hardening rule and based on the maximum of the increasing phase of the stabilized cycle (also called a 'quarter-cycle approach' or 'half range strain assessment'). This method has a restricted validity domain; it is only applicable in very simple symmetric loading with either zero or positive mean stress. Its use should be limited to configurations in which the maximum strain is reached during the first quarter cycle and justified on a case-by-case basis.

ASME III (20) and RCC-M paragraph §B3234.2 (12) allow analysts to use the average of the tabulated design stress intensity S_m at the maximum and minimum temperatures of the cycle when computing the K_e factor for cyclic thermal loading. These tabulated values are nominally mean values. However if the stress is driven by the thermal loading, the values can only be the average between the maximum and minimum temperatures of the cycle. In the case of a pressure variation at high temperature, the use of an average S_m is unconservative. In the absence of any additional justification and independent material properties over the temperature range in question (isotherm constant value) the temperature that maximizes the stress or strain range is considered. In a non-linear analysis, it is therefore recommended that to be more realistic, anisothermal material properties are employed.

The method described below is used to determine the maximum total strain range for each studied combination of transients. The concept of transient fictive 1 and fictive 2, and the definition of main cycles and sub-cycles of the linear fatigue analysis is still applicable here for the non-linear analysis.

The analysis of the total strain amplitudes (calculated in tensor form) uses a notion of equivalent strain range which can be determined either according to Tresca, or von Mises depending on analysts' choice of code.

5.2 Tensor notations

The strain and stress range tensors used are as follows:

- $\Delta\varepsilon_{ij}^{t}$, $\Delta\varepsilon_{ij}^{e}$ and $\Delta\varepsilon_{ij}^{p}$ are respectively the total strains, the elastic strains, and the plastic strains of the 'difference' tensor of strains between two calculation instants.
- $\Delta\varepsilon_{i}^{t}$, $\Delta\varepsilon_{i}^{e}$ and $\Delta\varepsilon_{i}^{p}$ are respectively the total principal strains, the elastic principal strains and the plastic principal strains of the 'difference' tensor of strains between two calculation instants.
- $\Delta\sigma_i$ are the principal stresses in the principal coordinate system of the 'difference' tensor of stresses between two calculation instants.

5.3 Approach A: direct elastic-plastic analysis

Two methods to calculate equivalent total strain range are provided: either from the total strain tensor (method 1) or by partitioning the elastic strain range from the plastic strain range (method 2). These two methods are equivalent and acceptable.

The formulations presented below consider the incompressibility (ν=0.5) in the plastic domain and the effective Poisson ratio in the elastic domain.

It should be noted that for the two methods in the ASME code, the shear engineering strain γ is employed, whereas in RCC-M the tensorial shear strain components ε are preferred. The two formulations are equivalent and consistent however as shown in Equation 37 below. The subsequent sections make use of the RCC-M approach.

$$\underline{\underline{\boldsymbol{\varepsilon}}} = \begin{bmatrix} \varepsilon_{xx} & \varepsilon_{xy} & \varepsilon_{xz} \\ \varepsilon_{yx} & \varepsilon_{yy} & \varepsilon_{yz} \\ \varepsilon_{zx} & \varepsilon_{zy} & \varepsilon_{zz} \end{bmatrix} = \begin{bmatrix} \varepsilon_{xx} & \frac{1}{2}\gamma_{xy} & \frac{1}{2}\gamma_{xz} \\ \frac{1}{2}\gamma_{yx} & \varepsilon_{yy} & \frac{1}{2}\gamma_{yz} \\ \frac{1}{2}\gamma_{zx} & \frac{1}{2}\gamma_{zy} & \varepsilon_{zz} \end{bmatrix}$$

Equation 37

5.3.1 Method 1: calculation of an equivalent total strain from a total strain tensor

For a given point and for a pair of instants, the equivalent total elastic-plastic strain range $\Delta\varepsilon_t$ to be considered for the fatigue assessment is computed from the equivalents according to Tresca or von Mises as follows:

$$\Delta\varepsilon_t = \Delta\varepsilon^t_{eq,(VM,Tresca)} + \frac{1-2\nu}{3}\frac{\Delta\sigma_{eq,(VM,Tresca)}}{E}$$

Equation 38

with:

$\Delta\varepsilon^t_{eq,Tresca}$: the equivalent total strain range according to Tresca:

$$\Delta\varepsilon^t_{eq.Tresca} = \frac{2}{3}Max(|\Delta\varepsilon^t_1 - \Delta\varepsilon^t_2|, |\Delta\varepsilon^t_2 - \Delta\varepsilon^t_3|, |\Delta\varepsilon^t_1 - \Delta\varepsilon^t_3|)$$

Equation 39

$\Delta\varepsilon^t_{eq,VM}$: the equivalent total strain range according to von Mises:

$$\Delta\varepsilon^t_{eq,VM} = \frac{\sqrt{2}}{3}[(\Delta\varepsilon^t_{11} - \Delta\varepsilon^t_{22})^2 + (\Delta\varepsilon^t_{22} - \Delta\varepsilon^t_{33})^2 + (\Delta\varepsilon^t_{33} - \Delta\varepsilon^t_{11})^2 + 6\{(\Delta\varepsilon^t_{12})^2 + (\Delta\varepsilon^t_{23})^2 + (\Delta\varepsilon^t_{31})^2\}]^{\frac{1}{2}}$$

Equation 40

$\Delta\sigma_{eq.Tresca}$: the equivalent stress range according to Tresca:

$$\Delta\sigma_{eq.Tresca} = Max(|\Delta\sigma_1 - \Delta\sigma_2|, |\Delta\sigma_2 - \Delta\sigma_3|, |\Delta\sigma_1 - \Delta\sigma_3|)$$

Equation 41

$\Delta\sigma_{eq.VM}$: the equivalent stress range according to von Mises:

$$\Delta\sigma_{eq.VM} = \sqrt{\frac{1}{2}[(\Delta\sigma_3 - \Delta\sigma_1)^2 + (\Delta\sigma_3 - \Delta\sigma_2)^2 + (\Delta\sigma_2 - \Delta\sigma_1)^2]}$$

Equation 42

It should be noted that as the total equivalent strain range $\Delta\varepsilon^t_{eq,Tresca}$ or $\Delta\varepsilon^t_{eq,Mises}$ is computed with ν=0.5 (valid only for the plastic domain), a correction for the elastic domain is added to take into account the elastic equivalent strain range $\Delta\sigma_{eq.Tresca}$ or $\Delta\sigma_{eq.VM}$ with the effective ν value instead of ν =0.5.

5.3.2 Method 2: calculation of an equivalent total from tensors of elastic strains and plastic strains

For a given point and for a pair of instants, the equivalent total elastic-plastic strain range $\Delta\varepsilon_t$ to be considered for the fatigue assessment is expressed as follows:

- According to Tresca:

$$\Delta\varepsilon_t = \frac{1}{1+\nu} Max(|\Delta\varepsilon_1^e - \Delta\varepsilon_2^e|, |\Delta\varepsilon_2^e - \Delta\varepsilon_3^e|, |\Delta\varepsilon_1^e - \Delta\varepsilon_3^e|) + \frac{1}{1.5} Max(|\Delta\varepsilon_1^p - \Delta\varepsilon_2^p|, |\Delta\varepsilon_2^p - \Delta\varepsilon_3^p|, |\Delta\varepsilon_1^p - \Delta\varepsilon_3^p|)$$

Equation 43

- According to von Mises:

$$\Delta\varepsilon_t = \frac{1}{1+\nu}\sqrt{\frac{1}{2}\left[(\Delta\varepsilon_{11}^e - \Delta\varepsilon_{22}^e)^2 + (\Delta\varepsilon_{22}^e - \Delta\varepsilon_{33}^e)^2 + (\Delta\varepsilon_{33}^e - \Delta\varepsilon_{11}^e)^2 + 6\left(\Delta\varepsilon_{12}^{e\,2} + \Delta\varepsilon_{23}^{e\,2} + \Delta\varepsilon_{31}^{e\,2}\right)\right]} + \frac{1}{1.5}\sqrt{\frac{1}{2}\left[\left(\Delta\varepsilon_{11}^p - \Delta\varepsilon_{22}^p\right)^2 + \left(\Delta\varepsilon_{22}^p - \Delta\varepsilon_{33}^p\right)^2 + \left(\Delta\varepsilon_{33}^p - \Delta\varepsilon_{11}^p\right)^2 + 6\left(\Delta\varepsilon_{12}^{p\,2} + \Delta\varepsilon_{23}^{p\,2} + \Delta\varepsilon_{31}^{p\,2}\right)\right]}$$

Equation 44

5.4 Approach B: elastic-plastic amplification assessment

5.4.1 Calculation of the elastic-plastic concentration factor K_e

The parameter K_e is equal to the ratio between the elastic-plastic strain range and the value calculated in the elastic hypothesis. K_e should therefore be deduced from two calculations: an elastic one and elastic-plastic one. For both calculations, the equivalent stresses and strains are calculated according to the same equivalent (either according to Tresca or according to von Mises). For this assessment, a direct calculation according to approach A (see Section 4.3) must be carried out based on one of the two methods proposed (direct calculation of the equivalent total strain from an elastic-plastic calculation).

$$K_e = \frac{\Delta\varepsilon_t(elastic - plastic\ calculation)}{\Delta\varepsilon_t(elastic\ calculation)}$$

Equation 45

The term $\Delta\varepsilon_t$ *(elastic-plastic calculation)* is the one defined in Section 5.3.

The term $\Delta\varepsilon_t(elastic\ calculation)$ is defined:

- According to Tresca:

$$\Delta\varepsilon_{t_{(elastic)}} = \frac{1}{1+\nu} Max(|\Delta\varepsilon_1^e - \Delta\varepsilon_2^e|, |\Delta\varepsilon_2^e - \Delta\varepsilon_3^e|, |\Delta\varepsilon_1^e - \Delta\varepsilon_3^e|)$$

Equation 46

- According to von Mises:

$$\Delta\varepsilon_{t_{(elastic)}} = \frac{1}{1+\nu}\sqrt{\frac{1}{2}\left[(\Delta\varepsilon_{11}^e - \Delta\varepsilon_{22}^e)^2 + (\Delta\varepsilon_{22}^e - \Delta\varepsilon_{33}^e)^2 + (\Delta\varepsilon_{33}^e - \Delta\varepsilon_{11}^e)^2 + 6\left(\Delta\varepsilon_{12}^{e\ 2} + \Delta\varepsilon_{23}^{e\ 2} + \Delta\varepsilon_{31}^{e\ 2}\right)\right]}$$

Equation 47

It is recommended that in the case of an analysis with a temperature dependent modulus of elasticity, the value that maximizes parameter K_e should be chosen.

5.4.2 Generalization of the elastic-plastic concentration factor

For conditions of combined mechanical and thermal loading, a global K_e can be assessed.

The elastic-plastic correction K_e determined for a given combination of conditions can be partially generalized to loading conditions of the same type as that considered in the non-linear calculation and whose intensity is bounded by the retained combination of conditions (for example, thermal shocks with longer shock duration or a lower temperature range than those considered in the calculation).

For complex loading conditions, a sensitivity study must be carried out to demonstrate the conservative character of the chosen solution and to limit its applicability.

Within an analysis, several values of K_e can be used to deal with several groups of conditions. The calculation of K_e from equivalents of Tresca or of von Mises are very similar; both approaches are therefore acceptable.

5.5 Plasticity model

The isotropic hardening model does not take into consideration the Bauschinger effect. Any FEA results obtained beyond the first stress reversal are essentially hypothetical (*i.e.*, underprediction of full-cycle strain range, see Benchmark 2.1 in (1)). This model is therefore not valid for cyclic loads.

A non-linear kinematic hardening rule (such as Armstrong-Frederick model, Chaboche model or combined strain hardening rule) should be used instead.

The general expression of these models is described below.

The plasticity criterion is expressed by:

$$f(\boldsymbol{\sigma}, \mathbf{X}, R) = | \boldsymbol{\sigma} - \mathbf{X} | - R - \sigma_y = 0$$

Equation 48

where:

σ: stress tensor.

R: scalar parameter for the isotropic strain hardening part, representing the expansion of the yield surface (see Figure 24).

X: tensor component for the kinematic strain hardening part (back stress tensor) representing the translation of the yield surface (see Figure 25).

σ_y: initial tensile yield strength. Generally, the value of σ_y is lower than the conventional $R_{P0.2}$ offset yield strength.

The non-linear kinematic strain hardening is expressed as follows:

$$X = \sum_{i=1}^{n} X_i$$

Equation 49

$$\delta X_i = \frac{2}{3} C_i \delta \varepsilon^p - \gamma_i X_i |\delta \varepsilon^p|$$

Equation 50

where:

n: number of back stress components for the kinematic hardening

C, γ: kinematic hardening material parameters

$\delta \varepsilon^p$: increment of plastic strain

The isotropic strain hardening evolution is as follows:

$$\delta R = b(Q - R)|\delta \varepsilon^p|$$

Equation 51

where:

b, Q: constants of the material, which have the effect of introducing progressive cyclic hardening (or softening)

The simplest constitutive law for non-linear fatigue analysis is the Armstrong-Frederick model which uses only one non-linear kinematic component $(n=1)$. The number of parameters is then reduced to three (γ_1, C_1 and σ_y) and the identification process could be carried out analytically. With this simple model, there is no progressive cyclic hardening/softening modelling.

It is therefore recommended that the parameter identification should be performed in a conservative way either on the monotonic strain-stress curve or on the reduced cyclic curve. Care should also be taken in the way the C and γ parameters are fitted to represent the stress-strain curve. Compromises need to be made regarding the target strain domain as only one kinematic component is defined.

The superposition of two or three kinematic components (n=2 or n=3) is usually selected to obtain a reasonably accurate representation of all the strain domains. The identification process sometimes requires an optimization algorithm, but this is not very costly in terms of computation.

The models previously presented are temperature-independent. In case of discrete parameter identifications at different temperatures, extra care should be taken in the way the coefficients are interpolated with respect to temperature. If only one of the material coefficients does not change in a monotonic way with temperature, the interpolation becomes false.

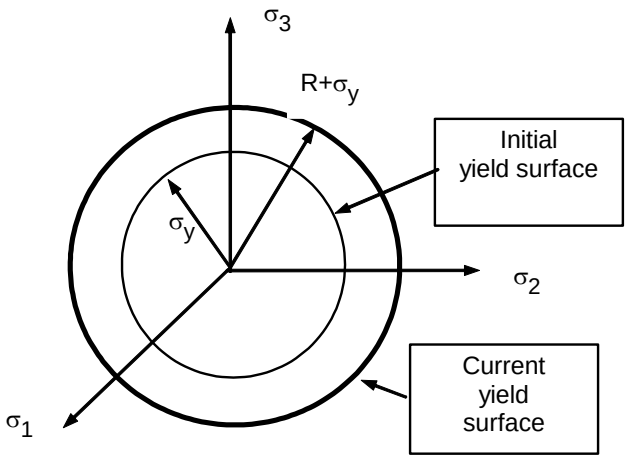

Figure 24. Representation of the isotropic strain hardening

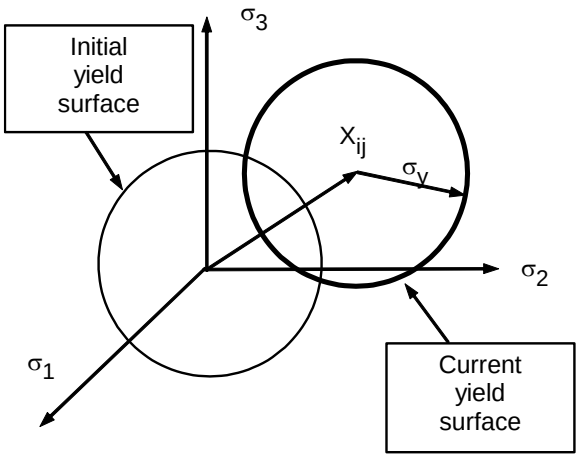

Figure 25. Representation of the kinematic strain hardening

5.6 Material data

The material data, required for the implementation of kinematic (or combined) strain hardening for the non-linear fatigue analyses, are at least the monotonic tensile curves and the cyclic strain hardening curves.

Monotonic tensile curves are available in some codes (RSE-M, RCC-MRx). RCC-MRx also provides cyclic curves for several materials. As an alternative to the material data available in the codes, it is possible to use material data of the corresponding manufacturer file or specific test campaign, subject to sufficient justification (enough tests, representative samples, variation in temperature, *etc*.).

6. Conclusions

This report built upon the findings of the preceding reports in the CORDEL *Non-Linear Analysis Design Rules* series to explore the areas in which the benchmark problems identified a need for consensus in design codes to propose recommendations for harmonization. A summary of the recommendations for each step of non-linear analysis methods is presented within this conclusion.

Linear mechanical analysis

Guidance has been lacking for linear mechanical analysis as it is sometimes believed to be straightforward and well understood. Currently practices are not satisfactory when treating complex shapes with discontinuity areas. This report offers some guidelines for dealing with such scenarios which could be further developed within design codes. The guiding principle for undertaking the analysis is to perform sensitivity runs until convergence is reached to establish control of the calculation's parameters. The rules for the classification of stress (primary or secondary) could also be harmonized between codes where possible.

For linear mechanical analysis, three categories of stress are defined in nuclear codes: membrane, membrane + bending, and peak, as well as the damages that these stresses produce. The damages that were discussed were excessive deformation and plastic instability. The section provided recommendations to aid analysts with the initialization of their modelling. Geometric choices have a considerable impact on both the accuracy of results and the computation time. It was therefore recommended to split large components into distinct zones for faster calculation where possible while ensuring that boundary conditions match and that discontinuities are appropriately managed. In the case of asymmetric geometries, a minimum recommended distance between boundaries and discontinuities is presented in Section 2.1.3.

Recommendations were also made to assist analysts with their choice between a 2D or 3D model. These are presented in Table 6 below.

Table 6. Comparison of 2D and 3D modelling

	Advantages	**Drawbacks**
2D Model	Faster computation Straightforward to interpret results	Lack of stress or strain in third dimension Forced approximation for certain geometries Inability to apply some loads with all tensor components
3D Model	Precise and detailed results Complete tensors can be applied Realistic geometries	Slower computation Obtaining results is more difficult as an area to analyse must be chosen

Accurate modelling results require an astute selection of the FEA mesh applied to the geometry. Several elements are typically at the disposal of analysts (solid, shell, beams *etc*.) but their choice must be consistent with the behaviour of the structure and the domain in which the elements are valid. The density of the mesh and variations in density are also important choices which not only affect the accuracy of the results but also the computation time. It is recommended that the density should be increased when approaching discontinuity zones where stresses concentrate while ensuring that the mesh is fine enough to capture bending stress gradients through the model in zones away from discontinuities. When thermal loads are being considered, the analyst should ensure that the meshing density is increased through the thickness towards surfaces. The selection of time discretization must also ensure that the thermal field is stable and avoids temperature oscillations.

Following the computation, the stresses revealed by the computation are post-processed. Two aspects of post-processing that are of particular importance are defining stress classification lines and linearizing stresses. The definition of cross-sections is crucial as the stresses present in these sections are directly compared to the allowable stresses in codes and standards. Maximum stress values must be captured within line segments, but it should be noted that the maximum stresses are not always at the same point. It is recommended that certain special locations be therefore treated differently as FEA calculations can be affected by stress classification lines that contain a singularity. It is therefore important to linearize the stresses appropriately. Recommendations for this procedure are presented in Section 2.2.3 for through-thickness stress and shear stresses. Stress analysis is covered in the final part of the linear mechanical analysis section, which presents recommendations for the classification of stresses within the model. Analysts much verify triaxiality criteria and other categories of stress to check for excessive deformation and plastic instability.

Plastic analysis

The design codes offer the possibility to assess plastic collapse using limit load and double slope methods which provide consistent results as long as consistent material data is used. This was observed through the benchmarking performed in the preceding reports (1) (2). Guidance is required for the choice of flow stress for plastic instability which is not currently provided in most design codes. Maximum local strain methods are not proposed in design codes as these are very sensitive to the maximum strain value and the post-processing of FEA results.

For plastic analysis, several methods for calculating collapse loads were presented (limit load, double slope, and maximum strain 0.5%) along with recommendations for performing each type as seen in Figure 1 and Figure 2. A series of recommendations for the maximum strain 0.5% method are also provided. It was noted that the limit load analysis assumes an elastic-perfectly plastic material and as such is less practical and instructive than the elastic-plastic stress analysis. Plastic instability is covered next, identifying the von-Mises yield function as a better choice than Tresca for metallic materials as it does not include any singularities in its formulation.

Elastic fatigue analysis

Guidance for elastic fatigue problems is issued in the following section with clear recommendations for the linearization of stresses in such scenarios. Firstly, the linearization should be performed at each time-step and not only for those that feature extreme stresses. Secondly the time-steps used for both thermal and mechanical analysis should be adequately refined during the loading event and following it for long enough to capture the maximum P+Q

stress. Finally, the calculation of membrane and bending stress resultants should be performed for all the unique stress components by default. Recommendations for cyclical fatigue analysis are then put forward following coverage of the static scenarios. To ensure appropriately conservative results, the S_p and S_n for each counted cycle should be determined independently for calculating K_e and S_{alt}. Material properties are then examined as these have a considerable influence on the results of fatigue calculations. A straightforward approach for obtaining the design stress intensity, S_m, is presented based upon the RCC-M and ASME code requirements in Section 0 which has the advantage of being more meaningful and being compatible with most cycle counting algorithms. It should be noted that this approach is for selecting the most appropriate temperature to set the value of S_m for the plasticity correction factor and that S_m is not a FEA result. Two options for the calculation of the representative elastic modulus are recommended in Section 0 due to their ability to reduce the conservatism within fatigue calculations. As previously mentioned for static loads, the properties accorded to a material during analysis significantly impact the results of a simulation. This is no different for cyclical loads, and it is therefore recommended that temperature-dependent material properties should be employed for stress analysis where possible. Fixed temperature properties do have their place however, if analysts are aiming to maximize stress for example. In this case, is it recommended that analysts undertake sensitivity studies to understand the competing effects of various material properties on the fatigue damage.

Harmonization across design codes for some aspects of elastic fatigue analysis is currently underway, notably for the K_e factor however other areas still require further examination and comparison work such as cycle counting for example. CORDEL will be covering these topics in a future publication on Fatigue Life Analysis, in close cooperation with the SDOs.

Plastic fatigue analysis

The final section covering plastic fatigue analysis presents two different approaches to the topic. The first of which uses a direct analysis to obtain the ranges of elastic-plastic strain while the second one uses an elastic-plastic concentration factor K_e, which is employed when the yield strength of a material is exceeded to refine plastic corrections in the linear fatigue analysis. In both cases, material properties play an important role and similarly to recommendations in the elastic fatigue analysis section, it is best practice to employ anisothermal material properties to reduce conservatism despite the increased complexity. The second approach is of greater interest due to the recommendations for the K_e factor, which is the ratio of the elastic-plastic strain range to the elastic strain range. Both these ranges must be calculated themselves and the same method (Tresca or von Mises) must be employed for both. When the modulus of elasticity used in these calculations is a function of temperature, it is recommended that the value of the modulus that maximizes the K_e factor be used. In the case of complex loading conditions, it is recommended that analysts carry out a sensitivity study to ensure that the chosen solution is conservative and to provide the domain in which the solution is applicable. Plasticity models are discussed, stating that the isotropic hardening model does not consider the Bauschinger effect and therefore FEA results obtained following the first stress reversal cannot be relied upon for accuracy. It is therefore recommended that a non-linear kinematic hardening rule be employed instead. The Armstrong-Frederick model and the Chaboche model are suitable alternatives. It should be noted however for the Armstrong-Frederick model that compromises will need to be made with regard to the target strain domain as it only defines a single kinematic component.

It should be noted that while it is feasible to employ non-linear methods for plastic fatigue analysis, they can be challenging to implement in industrial practices. This is due to the amount of care required in determining appropriate parameters to fit the material cyclic behaviour and the considerable computational power require to perform the calculations.

Concluding remarks

The work and recommendations presented within this report are the culmination of two years of work by the MCSTF based upon the outcomes of code comparisons and benchmarking. The methods employed in some of the benchmarks are not codified but present insight into the possibilities offered by different approaches that the MCSTF recommends for examination by SDOs. The findings of the report also demonstrate the importance and influence of choices made by analysts during the post-processing of their non-linear analysis. The selection of post-processing parameters, notably for plastic instability, is an area in which standard operating procedures should be developed to ensure a consistent approach. The MCSTF will continue to build upon the work presented in this report, notably with regard to fatigue for which a subsequent report is currently under preparation.

References

1. *Non-Linear Analysis Design Rules Part 2a: Specification of Benchmarks on Nozzles under Pressure, Thermal and Piping Loads.* **World Nuclear Association**, 2019.
2. *Non-Linear Analysis Design Rules Part 2b: Assessment of Non-Linear Benchmark Results.* **World Nuclear Association**, 2020.
3. **Kalnins, Arturs.** *Stress Classification Lines Straight Through Singularities*, 2008.
4. *Prevention of damages in mechanical components - Introduction to the design, analysis and construction rules of the RCC-M.* **AFCEN**, 2014.
5. *BPVC Section VIII - Rules for Construction of Pressure Vessels Division 2 - Alternative Rules.* **ASME**, 2019.
6. *BPVC Section VIII-Rules for Construction of Pressure Vessels Division 1.* **ASME**, 2019.
7. *BPVC Section VIII-Rules for Construction of Pressure Vessels Division 3-Alternative Rules for Construction of High Pressure Vessels.* **ASME**, 2019.
8. **Marie, Stéphane.** *Analytical expression of the thermal stresses in a vessel or pipe with cladding submitted to any thermal transient.* 4, s.l. : International Journal of Pressure Vessels and Piping, 2004, Vol. 81.
9. *BPVC Section VIII-Rules for Construction of Pressure Vessels Division 2-Alternative Rules.* **ASME**, 2019. 9780791872888.
10. *RCC-MRX Design and Construction Rules for mechanical components of nuclear installations : high-temperature, research and fusion reactors.* **AFCEN**, 2018.
11. **Hollinger, J. L. and Hechmer G. L.** *3D stress criteria guidelines for application.* WRC bulletin, 1998, Vol. 429.
12. *RCC-M: Design and Construction Rules for Mechanical Components of PWR Nuclear Island.* **AFCEN**, 2015.
13. *BPVC Section II-Materials-Part D-Properties-(Customary).* **ASME**, 2019. 9780791872703.
14. *ASME Record 17-924: Allowable Alternative Fatigue Design Curves for Austenitic Steels and Ferritic Steels with UTS ≤ 80 ksi.* **ASME**, 2020.
15. **Manjoine, M.J. and Tome, R.E.** *Proposed Design Criteria for High Cycle Fatigue of Stainless Steels, International Conference on Advances in Life Prediction, Methods, pp. 51-57.* ASME, 1983.
16. **Ranganath, S.** *BWRVIP-322: BWR Vessel and Internals Project, Revised Allowable High-Cycle Fatigue Design Curves for Austenitic and Ferritic Steels, Report No. 3002014859.* s.l. : EPRI, 2019.
17. **Jaske, C. and O'Donnell, W.J.** *Fatigue Design Criteria for Pressure Vessel Alloys.* 4, s.l. : J. Pressure Vessel Technol., 1977, Vol. 99.
18. **Gilman, Tim.** *Stress-Based Fatigue Monitoring: Methodology for Fatigue Monitoring of Class 1 Nuclear Components in a Reactor Water Environment.* EPRI, 2012.
19. *BPVC Section III-Rules for Constructions of Nuclear Facility Components-Subsection NCA-General Requirements for Division 1 and Division 2.* **ASME**, 2019. 9780791872727.

World Nuclear Association
Tower House
10 Southampton Street
London WC2E 7HA
United Kingdom

+44 (0)20 7451 1520
www.world-nuclear.org
info@world-nuclear.org

Major design rules in pressure vessel and piping codes are based on the linear elastic approach, which uses stress classification. This approach becomes impractical, however, for complex geometry and load combinations. The use of non-linear analysis at design level is an efficient alternative to the linear elastic approach as it is based on real material behaviour and more accurate deformation criteria and negates the need for stress classification.

Non-Linear Analysis Design Rules Part 3: Recommendations for Industrial Practices is the final report in a series on non-linear analysis design rules, which is built on the assessment of international non-linear analysis benchmark results. It proposes recommendations for industrial practices in non-linear analysis of safety grade reactor components from the initial setting of parameters to the post-processing and interpretation of results. These results are comprised of linear mechanical analysis, plastic analysis, elastic fatigue analysis, and plastic fatigue analysis. The report also recommends that Standard Developing Organizations consider the report's proposed practices as the basis of future harmonization efforts across mechanical codes and standards.

This report has been produced by the Mechanical Codes and Standards Task Force of the World Nuclear Association's Cooperation in Reactor Design Evaluation and Licensing (CORDEL) Working Group.